Fusion pore regulation by cAMP/Epac2 controls cargo release during insulin exocytosis

Alenka Gucek[1], Nikhil R Gandasi[1], Muhmmad Omar-Hmeadi[1], Marit Bakke[2], Stein O. Døskeland[2], Anders Tengholm[1], and Sebastian Barg[1,*]

1 Department of Medical Cell Biology
BMC Box 571, Uppsala University
75123 Uppsala, Sweden
2 Department of Biomedicine
University of Bergen
Bergen, Norway
*** Correspondence** (*sebastian.barg@mcb.uu.se*, +46-18 4714660)

Abstract:

Regulated exocytosis establishes a narrow fusion pore as initial aqueous connection to the extracellular space, through which small transmitter molecules such as ATP can exit. Co-release of polypeptides and hormones like insulin requires further expansion of the pore. There is evidence that pore expansion is regulated and can fail in diabetes and neurodegenerative disease. Here we report that the cAMP-sensor Epac2 (Rap-GEF4) controls fusion pore behavior by acutely recruiting two pore-restricting proteins, amisyn and dynamin-1, to the exocytosis site in insulin-secreting beta-cells. cAMP elevation restricts and slows fusion pore expansion and peptide release, but not when Epac2 is inactivated pharmacologically or in Epac2$^{-/-}$ (*Rapgef4*$^{-/-}$) mice. Consistently, overexpression of Epac2 impedes pore expansion. Widely used antidiabetic drugs (GLP-1 receptor agonists and sulfonylureas) activate this pathway and thereby paradoxically restrict hormone release. We conclude that Epac2/cAMP controls fusion pore expansion and thus the balance of hormone and transmitter release during insulin granule exocytosis.

Keywords: fusion pore; exocytosis; Epac2; RapGef4; secretory granule; hormone secretion; cAMP; tolbutamide; GLP-1; exendin-4

Introduction

Insulin is secreted from pancreatic β-cells and acts on target tissues such as muscle and liver to regulate blood glucose. Secretion of insulin occurs by regulated exocytosis, whereby secretory granules containing the hormone and other bioactive peptides and small molecules fuse with the plasma membrane. The first aqueous contact between granule lumen and the extracellular space is a narrow fusion pore (upper limit 3 nm [1]) that is thought to consist of both lipids and proteins [2,3]. At this stage, the pore acts as a molecular sieve that allows release of small transmitter molecules such as nucleotides and catecholamines, but traps larger cargo [4–7]. Electrophysiological experiments have shown that the fusion pore is short-lived and flickers between closed and open states, suggesting that mechanisms exist that stabilize this channel-like structure and restrict pore expansion [6,8–10]. The pore can then expand irreversibly (termed full fusion), which leads to mixing of granule and plasma membrane and release of the bulkier hormone content [4,5,11]. Alternatively, the pore can close indefinitely to allow the granule to be retrieved, apparently intact, into the cell interior (termed kiss-and-run or cavicapture) [4,6,12–14]. Estimates in β-cells suggest that 20-50% of all exocytosis in β-cells are transient kiss-and-run events that do not lead to insulin release [4,6]. However, kiss-and-run exocytosis contributes to local signaling within the islet because smaller granule constituents, such as nucleotides, glutamate or GABA, are released even when the fusion pore does not expand. Within the islet, ATP synchronizes β-cells [15], and has both inhibitory [16,17] and stimulatory [18] effects on insulin secretion. Within the islet, ATP suppresses glucagon release from α-cells [19], and activates macrophages [20]. Interstitial GABA leads to tonic GABA-A receptor activation and α-cell proliferation [21,22], and glutamate stimulates glucagon secretion [23].

Regulation of fusion pore behavior is not understood mechanistically, but several cellular signaling events affect both lifetime and flicker behavior. Pore behavior has been shown to be regulated by cytosolic Ca^{2+}, cAMP, PI(4,5)P2, and activation of protein kinase C (PKC) [6,8,24–26] and recent superresolution imaging indicates that elevated Ca^{2+} and dynamin promote pore closure [14,27]. Both myosin and the small GTPase dynamin are involved in fusion pore restriction [28–32], and assembly of filamentous actin promotes fusion pore expansion [33], suggesting a link to endocytosis and the cytoskeleton. In β-cells of type-2 diabetics, upregulation of amysin leads to decreased insulin secretion because fusion pore expansion is impaired [34], and the Parkinson's related protein α-synuclein promotes fusion pore dilation in chromaffin cells and neurons [35], thus providing evidence for altered fusion pore behavior in human disease.

Inadequate insulin secretion in type-2 diabetes (T2D) is treated clinically by two main strategies. First, sulfonylureas (e.g., tolbutamide and glibenclamide) close the K_{ATP} channel by binding to its regulatory subunit SUR1, which leads to increased electrical activity and Ca^{2+}-influx that triggers insulin secretion [36]. Sulfonylureas are given orally and are first line treatment for type-2 diabetes in many countries. Second, activation of the receptor for the incretin hormone glucagon-like peptide 1 (GLP-1) raises cytosolic [cAMP] and thereby increases the propensity of insulin granules to undergo exocytosis. Both peptide agonists of the GLP-1 receptor (e.g., exendin-4) and inhibitors of DPP-4 are used clinically for this purpose. The effect of cAMP on exocytosis is mediated by a protein-kinase A (PKA) dependent pathway, and by Epac2, a guanine nucleotide exchange factor for the Ras-like small GTPase Rap [37] that is a direct target for cAMP [38] and is recruited to insulin granule docking sites [39]. Epac2 has also been suggested to be activated by sulfonylureas [40], which may underlie some of their effects on insulin secretion.

Here we have studied fusion pore regulation in pancreatic β-cells, using high resolution live-cell imaging. We report that activation of Epac2, either through GLP1-R/cAMP signaling or via sulfonylurea, restricts expansion of the insulin granule fusion pore by recruiting dynamin and amisyn to the exocytosis site. Activation of this pathway by two classes of antidiabetic drugs therefore hinders full fusion and insulin release, which is expected to reduce their effectiveness as insulin secretagogues.

Results

cAMP-dependent fusion pore restriction is regulated by Epac but not PKA

To monitor single granule exocytosis, human pancreatic β-cells were infected with adenovirus encoding the granule marker NPY-Venus and imaged by TIRF microscopy. Exocytosis was evoked by local application of a solution containing 75 mM K^+, which leads to rapid depolarization and Ca^{2+} influx. Visually, two phenotypes of granule exocytosis were observed. In the first, termed full fusion, fluorescence of a granule that was stably situated at the plasma membrane suddenly vanished during the stimulation (in most cases within <100 ms; Fig 1a-c, left panels). Since the EGFP label is relatively large (3.7 nm vs 3 nm for insulin monomers) this is interpreted as rapid pore widening that allowed general release of granule cargo. The sudden release of material may suggest that this release coincided with the collapse of the granule into the plasma membrane , but we cannot exclude that at least some granules remained intact [12,14,29,41]. In the second type, the rapid loss of the granule marker was preceded by an increase in its fluorescence that could last for several seconds (flash

events, Fig 1a-c, right panels). We and others have previously shown [12,42,43] that this reflects neutralization of the acidic granule lumen and dequenching of the EGFP-label, before the labeled cargo is released. Since this neutralization occurs as the result of proton flux through the fusion pore, the fluorescence timecourse of these events can be used to quantitatively study fusion pore behavior.

In the following, we will report two parameters that reflect fusion pore behavior, the fraction of exocytosis events with flash phenotype (indicating restricted pores, about 40% in control conditions; Fig 1d), and the duration of the flash, referred to as "NPY release times". The latter was estimated by fitting a discontinuous function to the fluorescence timecourse (see Fig 1c, lines and Fig 1e), which limits the analysis to granules that eventually released their peptide content. The distribution of the NPY release times followed a mono-exponential function and was on average 0.87±0.12 s (186 granules in 26 cells) in control conditions (Fig 1e). Such events are increased by elevated cAMP [6,8] and likely other conditions that stabilize the fusion pore. Indeed, when forskolin (2 μM; fsk) was added to the bath solution we observed a 2-fold increase of exocytosis rate (Fig 1f), a 3-fold increase of NPY release times (Fig 1e), and a nearly doubled fraction of events with restricted fusion pores (Fig 1d,f). The GLP-1 agonist exendin-4 (10 nM; Ex4) had comparable effects (Fig 1d-f). Effects similar to those observed for human β-cells (Fig 1) were observed in the insulin secreting cell line INS-1 (Fig 1-Figure Supplement 1).

The effect of fsk on fusion pore behavior was mimicked by the specific Epac2 agonist S223 [44]. Incubation with S223-acetomethoxyester (5μM) increased the fraction of flash events by 60% (Fig 1d), doubled average NPY release times (Fig 1e) and doubled the event frequency (Fig 1f); the effects of fsk and S223 were not additive. In contrast, the Epac-inhibitor ESI-09 decreased the exocytosis rate in the presence of fsk by 80% (Fig 1f), and the average NPY release time and the fraction of flash events were both reduced by 60% (Fig 1d-e). PKA inhibition with Rp8-Br-cAMPS [45] decreased neither the fraction of flash events, nor average NPY release times (Fig 1e). The results indicate that Epac rather than PKA is responsible for cAMP-dependent fusion pore regulation. Paradoxically, Epac activation increases the rate of exocytosis but slows the rate of peptide release from individual granules.

Epac2 overexpression restricts fusion pores and prolongs their lifetime

We studied the effect of Epac2 overexpression on fusion pore regulation. INS-1 cells were co-transfected with EGFP-Epac2 and NPY-tdmOrange2 and fluorescence was recorded simultaneously in both color channels. Epac2 overexpression had no effect on the overall exocytosis rate in either absence or presence of fsk (Fig 2a), but increased the rate of flash events (Fig 2b-c), supporting our finding, based on manipulation of the endogenous Epac2 activity, that Epac2 is involved in fusion pore regulation (Fig 1d). NPY release times in cells overexpressing Epac2 increased 3-fold in the absence of fsk, and were similar to controls in presence of fsk (Fig 2d). This indicates that a high Epac concentration can achieve sufficient activity to affect insulin secretion even at basal cAMP level, likely because cAMP acts in part by increasing the Epac concentration at the plasma membrane [39].

ATP release is accelerated upon Epac inhibition

To test if cAMP-dependent fusion pore restriction affects release of small transmitter molecules, we quantified nucleotide release kinetics from individual granules using patch clamp electrophysiology. The purinergic receptor cation channel $P2X_2$, tagged with RFP ($P2X_2$-RFP), was expressed in INS-1 cells as an autaptic nucleotide sensor [4] (Fig 3a). The cells were voltage-clamped in whole-cell mode and exocytosis was elicited by including a solution with elevated free Ca^{2+} (calculated 600 nM) in the patch electrode. In this configuration, every exocytosis event that co-releases nucleotides causes an inward current spike, similar to those observed by carbon fiber amperometry (Fig 3a-b). Including cAMP in the pipette solution doubled the frequency of current spikes, consistent with accelerated exocytosis. This effect of cAMP was blocked if the Epac inhibitor ESI-09 was present (Fig 3b-c). The current spikes (see Fig 3a, right) reflect nucleotide release kinetics during individual exocytosis events. In the presence of cAMP, but not cAMP+ESI-09, they were markedly widened as indicated by on average 20% longer half-widths (Fig 3d), 30% longer decay constants (τ, Fig 3e), and 40% slower rising phases (25-75% slope, Fig 3f), compared with control. This indicates that nucleotide release is slowed by cAMP, likely because of changed fusion pore kinetics. Since the effect is blocked by ESI-09, we conclude that the cAMP effect probably is mediated by Epac.

cAMP-dependent fusion pore regulation is absent in Epac2$^{-/-}$ (*Rapgef4*$^{-/-}$) β-cells

Since ESI-09 blocks all Epac isoforms[46], we characterized fusion pore behavior in isolated β-cells from Epac2$^{-/-}$ (*Rapgef4*$^{-/-}$) mice that lack all splice variants of Epac2 [47]. Cells from WT or Epac2$^{-/-}$ mice were infected with

adenovirus encoding the granule marker NPY-tdmOrange2 and challenged with 75 mM K^+ (Fig 4a-b). In the absence of forskolin, exocytosis was significantly slower in Epac2$^{-/-}$ cells than WT cells, and the fraction of flash-associated exocytosis events was five-fold lower (Fig 4c-e). This was paralleled by strikingly shorter fusion pore life-times in Epac2$^{-/-}$ cells compared with WT (Fig 4f). The data suggest that Epac2 is partially activated in these conditions, consistent with elevated cAMP levels in mouse β-cells in hyperglycemic conditions [48]. As expected, forskolin increased both exocytosis (Fig 4e) and the fraction of flash events (Fig 4c) of WT cells. In contrast, forskolin failed to accelerate exocytosis in Epac2$^{-/-}$ cells, and the fraction of flash events was similar with or without forskolin (Fig 4c, f-g). We conclude therefore that the effects of cAMP on fusion pore behavior are mediated specifically by Epac2.

Sulfonylureas delay fusion pore expansion through the same pathway as cAMP

Sulfonylureas have been reported to activate Epac [40], in addition to their classical role that involves the sulfonylurea receptor (SUR). We therefore tested the effect of sulfonylureas on fusion pore behavior. INS-1 cells expressing NPY-tdmOrange2 were tested with three types of sulfonylureas, with different relative membrane permeability (tolbutamide<glibenclamide<gliclazide). In addition, diazoxide (200 μM) was present to prevent electrical activity. Exocytosis was not observed under these conditions, but could be triggered by local application of elevated K^+ (75 mM). In the absence of fsk, the sulfonylureas accelerated K^+-stimulated exocytosis about 2-fold over that observed in control (Fig 5b, left), which is consistent with earlier findings that sulfonylureas augment insulin secretion via intracellular targets [49]. This effect was entirely due to an increase in flash-associated exocytosis events (Fig 5b-c) and the average NPY release time increased accordingly in the presence of sulfonylurea (Fig 5d). Fsk strongly stimulated both flash-associated and full fusion exocytosis in absence of sulfonylurea (Fig 5b-c, middle); under these conditions sulfonylureas tended to decrease full-fusion exocytosis without effect on the frequency of flash-associated events (Fig 5b, middle). Accordingly, NPY release times were elevated compared with control (no fsk), and only marginally longer than with fsk alone (Fig 5d, right). Similar results were obtained in human β-cells, where glibenclamide increased exocytosis in the absence of fsk (P=0.01, n=13 cells from 4 donors) but not in its presence (P=0.80, n=7 cells from 4 donors; data not shown). The data indicate that sulfonylureas restrict fusion pore expansion through the same intracellular pathway as cAMP, which may counteract their stimulating effect on exocytosis by preventing or delaying peptide release.

Sulfonylureas also bind to SUR1 in the plasma membrane, which leads to rapid closure of K_{ATP} channels, depolarization and exocytosis. We tested the involvement of SUR1 by applying sulfonylureas acutely, which is expected to activate SUR1 in the plasma membrane but not Epac the cytosol (Fig 5e). Reduced diazoxide (50 μM) prevented glucose-dependent exocytosis but still allowed acute stimulation of exocytosis by sulfonylureas. Under these conditions, the fraction of flash-associated exocytosis events (Fig 5f-g) and the NPY release times (Fig 5h) was similar to control (stimulation with elevated K^+) for all three sulfonylureas. Taken together, the data suggest that sulfonylureas must enter the cytosol to affect fusion pore behavior, and that this effect is not mediated by the plasma membrane SUR. We excluded the possibility that sulfonylureas affect the fluorescence signal indirectly, by altering granule pH (Fig 5-Figure Supplement 1). Moreover, an EGFP-tagged SUR1 (EGFP-SUR1) expressed in INS-1 cells did not localize to exocytosis sites or affect fusion pore behavior (Fig 5-Figure Supplement 2). We therefore conclude that sulfonylureas affect fusion pore behavior through Epac2.

Dynamin and amisyn-controlled restriction of the fusion pore is cAMP-dependent

The proteins dynamin and amisyn have previously been implicated in fusion pore regulation in β-cells[29,34]. To understand how these proteins behave around the release site, we expressed EGFP-tagged dynamin1 (Fig 6a) or mCherry-tagged amisyn (Fig 6b) together with a granule marker in INS-1 cells, and stimulated exocytosis with elevated K^+. In the presence of fsk, both of the two fluorescent proteins were recruited to the granule site during membrane fusion (Fig 6c,f, & Fig 6-Figure Supplement 1). Expression of both proteins was about 2-4 fold compared with endogenous levels (Fig 6-Figure Supplement 2), and markedly increased the NPY release times (Fig 6d;g) and flash-associated exocytosis events (Fig 6e,h). Addition of the Epac inhibitor ESI09 prevented recruitment of both dynamin1 and amisyn during flash events and reduced flash events and NPY release times below control (Fig 6c-h). In the absence of fsk, expression of the two proteins had no effect on fusion pore behavior, and only amisyn (but not dynamin1) was recruited to the exocytosis site (Fig 6i-n). When Epac was activated with S223 (no fsk), dynamin1 and amisyn were recruited during flash events, and NPY release times and flash events were increased for both proteins (Fig 6i-n). The data suggest that dynamin1 and amisyn are acutely recruited to the exocytosis site, where they participate in cAMP-dependent fusion pore restriction.

Discussion

cAMP-dependent signaling restricts fusion pore expansion and promotes kiss-and-run exocytosis in β-cells [8] and neuroendocrine cells [25,50] (but see [51]). We show here that the cAMP-mediator Epac2 orchestrates these effects by engaging dynamin and perhaps other endocytosis-related proteins at the release site (Fig 7). Since the fusion pore acts as a molecular sieve, the consequence is that insulin and other peptides remain trapped within the granule, while smaller transmitter molecules with para- or autocrine function are released [4,6,12,52]. Incretin signaling and Epac activation therefore delays, or altogether prevents insulin secretion from individual granules, while promoting paracrine intra-islet communication that is based mostly on release of small transmitter molecules.

Paradoxically, two clinically important classes of antidiabetic drugs, GLP-1 analogs and sulfonylureas, activate Epac in β-cells and caused restriction of the fusion pore. Sulfonylureas have long been known to stimulate insulin secretion by binding to SUR1, which results in closure of K_{ATP} channels and depolarization [36]. The drugs also accelerate PKA-independent granule priming in β-cells, which may involve activation of intracellularly localized SUR1 [53]. Our data indicate that sulfonylureas exert a third mode of action that leads to the restriction of the fusion pore and therefore limits insulin release. Two pieces of evidence suggest that SUR1 is not involved in the latter. First, acute exposure to sulfonylureas had no effect on fusion pore behavior, although it blocks K_{ATP} channels (indicating SUR1 activation). Only long-term exposure to sulfonylurea resulted in restricted fusion pores, likely because it allowed the drugs to enter the cytoplasm. Second, we could not detect enrichment of SUR1 at the granule release site, which precludes any direct role of the protein in fusion pore regulation. Sulfonylurea compounds have been shown to allosterically stabilize the cAMP-dependent activation of Epac [54,55]. Our finding that sulfonylurea caused fusion pore restriction in the absence of forskolin indicates that basal cAMP concentrations are sufficient for this effect. Since gliclizide binds the CNB1 domain without activating it [54] and still restricts the fusion pore, Epac localization at the granule site [39] may be enough to regulate the downstream proteins (e.g. dynamin and amisyn). It can further be speculated that the competing stimulatory (via exocytosis) and inhibitor effects (via the fusion pore) of sulfonylureas on insulin secretion, contribute to the reduction in sulfonylurea effectiveness with time of treatment. Long term treatment with GLP-1 analogs disturbs glucose homeostasis [56], and combination therapy of sulfonylurea and DPP4 inhibitors (that elevate cAMP) has been shown to lead to severe hypoglycemia [57], an effect that likely depends on Epac [58].

Epac mediates the PKA-independent stimulation of exocytosis by cAMP [59] and our data suggests it may affect both priming and fusion pore restriction. This effect is rapid [53], suggesting that Epac is preassembled at the site of the secretory machinery. Indeed, Epac concentrates at sites of docked insulin granules [39], and forms functionally relevant complexes with the tethering proteins Rim2 and Piccolo [60]. However, the amount of Epac2 present at individual release sites did not correlate with fusion pore behavior, which may indicate that the protein acts indirectly by activating or recruiting other proteins. Indeed, we show here that recruitment of two other proteins, dynamin and amisyn, depends on cAMP and Epac. Other known targets of Epac are the small GTPases Rap1 and R-Ras, for which Epac is a guanine nucleotide exchange factor (GEF). Rap1 is expressed on insulin granules and affects insulin secretion both directly [61], and by promoting intracellular Ca^{2+}-release following phospholipase-C activation [62]. R-Ras is an activator of phosphoinositide 3-kinase [63]. By altering local phosphoinositide levels, Epac could therefore indirectly affect exocytosis via recruitment of C2-domain proteins such as Munc13 [64], and fusion pore behavior by recruitment of the PH-domain containing proteins dynamin and amisyn [65,66].

An unresolved question is whether pore behavior is controlled by mechanisms that promote pore dilation, or that instead prevent it. Dynamin causes vesicle fission during clathrin-dependent endocytosis [67], and since dynamin is present at the exocytosis site and required for the kiss-and-run mode [28,29,68], it may have a similar role during transient exocytosis. An active scission mechanism is also suggested by the finding that granules loose some of their membrane proteins during transient exocytosis [29,69]. Capacitance measurements have shown that fusion pores initially flicker with conductances similar to those of large ion channels, before expanding irreversibly [10]. This could result from pores that are initially stabilized through unknown protein interactions and that eventually give way to uncontrolled expansion. However, scission mechanisms involving dynamin can act even when the pore has dilated considerably beyond limit of reversible flicker behavior [14,70–72], and even relatively large granules retain their size during fusion-fission cycles [6,10]. Separate mechanisms may therefore operate, one that prevents pore dilation by actively causing scission, similar to the role of dynamins in endocytosis, and another by shifting the equilibrium between the open and closed states of the initial fusion pore. Curvature-sensitive proteins are particularly attractive for such roles since they could accumulate at the neck of the fused granule; such ring-like assemblies that have indeed been observed for the Ca^{2+}-sensor synaptotagmin [73]. Active pore dilation has also been proposed to be driven by crowding of SNARE proteins [74] and α-synuclein [35].

β-cell granules contain a variety of polypeptides (insulin, IAPP, chromogranins) and small molecule transmitter molecules (GABA, nucleotides, 5HT) that have important para- and autocrine functions within the islet [75,76]. Insulin modulates its own release by activating β-cell insulin receptors [77], stimulates somatostatin release [78], and inhibits glucagon secretion [79]. Insulin secretion is also inhibited by IAPP/amylin and chromogranin cleavage products such as pancreastatin [75]. Of the small transmitters, GABA inhibits glucagon secretion from α-cells [80] and enhances insulin secretion [81], and tonic GABA signaling is important for the maintenance of β-cell mass [81]. Adenine nucleotides cause β-cell depolarization, intracellular Ca^{2+}-release and enhanced insulin secretion [82,83], but also negative effects have been reported [16,17]. Paracrine purinergic effects also coordinate Ca^{2+} signaling among β-cells [15], stimulate secretion of somatostatin from δ-cells [84], and target islet vasculature and macrophages as part of the immune system [20]. By selectively allowing small molecule release, Epac/cAMP-dependent fusion pore restriction is expected to alter both the timing and the relative volume of peptidergic vs. transmitter signaling. Given that granule priming and islet electrical activity are regulated on a second time scale, even small delays between these signals can be envisioned to affect the ratio of insulin to glucagon secretion. As illustrated by the recent finding of altered fusion pore behavior in type-2 diabetes [34], Epac-dependent fusion pore regulation may have profound consequences for islet physiology and glucose metabolism in vivo.

Methods

Key resources table

REAGENT or RESOURCE	DESIGNATION	SOURCE OF REFERENCE	IDENTIFIERS	ADDITIONAL INFORMATION
strain, strain background (Adenovirus)	NPY-Venus	P Rorsman (Oxford)		
strain, strain background (Adenovirus)	NPY-tdmOrange2	this paper		See Constructs in Materials and Methods
Genetic reagent (*Mus musculus*)	*Rapgef4* KO and WT	Kopperud et al., 2017 [47]		
Cell line (*Rattus norvegicus domesticus*)	INS-1 Clone 832/12	Hohmeier et al., 2000 [85]	RRID:CVCL_7226	H Mulder (Malmö)

transfected construct (*Mus musculus*)	EGFP-Epac2	Idevall-Hagren et al., 2013 [86]	1068	
transfected construct (*Homo sapiens*)	NPY-tdmOrange2	Gandasi et al., 2015 [87]	1140	
transfected construct (*Rattus norvegicus*)	P2X2-mRFP1	Obermüller et al., 2005 [4]	1226	
transfected construct (*Homo sapiens*)	NPY EGFP mCherry	this paper		See Constructs in Materials and Methods
transfected construct (*Homo sapiens*)	Cherry2-amisyn	this paper	NM_001351940.1; 1286	See Constructs in Materials and Methods
transfected construct (*Homo sapiens*)	dynamin1-GFP	W Almers (Portland)	1342	
transfected construct (*Homo sapiens*)	NPY EGFP	W Almers (Portland)	1008	
Biological sample (*Homo sapiens*)	Human pancreatic islets	Goto et al., 2004 [88]		Nordic Network for Clinical Islet Transplantation Uppsala
Antibody	Rabbit polyclonal anti-amisyn	ab153974 abcam		1/50
Antibody	Rabbit monoclonal anti-dynamin1	ab52852 abcam	PMID:28171750	1/50
Chemical compound, drug	Cell dissociation buffer	Thermo Fisher	13150016	
Chemical compound, drug	Trypsin solution	Thermo Fisher	12604-021	
Chemical compound, drug	Lipofectamine 2000	Thermo Fisher	11668-019	
Chemical compound, drug	Forskolin ; Fsk	Sigma-Aldrich	F6886	
Chemical compound, drug	Polylysine	Sigma-Aldrich	P5899	
Chemical compound, drug	Exendin-4; Ex4	Anaspec (Fremont CA)	AS-24463	
Chemical compound, drug	Diazoxide	Sigma-Aldrich	D9035	
Chemical compound, drug	BSA	Sigma-Aldrich	F0804	

Chemical compound, drug	RPMI 1640	SVA	992680	
Chemical compound, drug	L-Glutamine	Hyclone	SH30034.01	
Chemical compound, drug	Tolbutamide ; tolb	Sigma-Aldrich	64-77-7	
Chemical compound, drug	Glibenclamide; glib	Hoechst		
Chemical compound, drug	Gliclizide; gliz	Sigma-Aldrich	21187-98-4	
Chemical compound, drug	S223	Biolog	B 056-01	
software, algorithm	MetaMorph	Molecular Devices		

Cells

Human islets were obtained from the Nordic Network for Clinical Islet Transplantation Uppsala [88] under full ethical clearance (Uppsala Regional Ethics Board 2006/348) and with written informed consent. Isolated islets were cultured free-floating in sterile dishes in CMRL 1066 culture medium containing 5.5 mM glucose, 10% fetal calf serum, 2 mM L-glutamine, streptomycin (100U/ml), and penicillin (100U/ml) at 37°C in an atmosphere of 5% CO_2 up to two weeks. Prior to imaging, islets were dispersed into single cells by gentle agitation using Ca^{2+}-free cell dissociation buffer (Thermo Fisher Scientific) supplemented with 10% (v/v) trypsin (0.05% Thermo Fisher Scientific). INS1-cells clone 832/13 [85] were maintained in RPMI 1640 (Invitrogen) with 10 mM glucose, 10% fetal bovine serum, streptomycin (100 U/ml), penicillin (100 U/ml), Sodium pyruvate (1 mM), and 2-mercaptoethanol (50 µM). The ins1 832/13 cells were screened by PCR and found negative for mycoplasma.

Mouse islets were isolated from 5-12 months old WT and Epac2$^{-/-}$ [47] (*Rapgef4*$^{-/-}$) animals. The Epac2 deletion involves exons 12-13, which include the high-affinity cAMP binding domain present in all Epac2 isoforms, in contrast to previously reported knockout strain [61], which only lacks the Epac2A isoform. The mice were anesthetized and the pancreas dissected out and cleared from fat and connective tissue in ice-cold Ca5 solution (in mM 125 NaCl, 5KCl, 1.2 $MgCl_2$, 1.28 $CaCl_2$, 10 HEPES; pH 7.4 with NaOH). Pancreas was injected with Collagenase P (1 mg/ml) and cut into small pieces before mechanical dissociation (7 min at 37 °C). BSA was added immediately and islets were washed 3X with ice cold Ca5 buffer with BSA. Islets were dispersed into single cells using Ca^{2+}-free cell dissociation buffer (supplemented with 10% (v/v) trypsin) and gentle agitation. Dispersed cells were sedimented by centrifugation, resuspended in RPMI 1640 medium (containing 5.5 mM glucose, 10% fetal calf serum, 100 U/ml penicillin and 100 U/ml streptomycin).

The cells were plated onto 22-mm polylysine-coated coverslips, and were transduced the next day using adenovirus (human & mouse cells) or transfected the same day with plasmids (INS1 cells, using Lipofectamine2000, Invitrogen) encoding the granule markers NPY-Venus, NPY-EGFP or NPY-tdOrange. Imaging proceeded 24-36 hours later.

Constructs

The open reading frame of human amisyn (NM_001351940.1) was obtained as a synthetic DNA fragment (Eurofins, Germany) and was cloned into pCherry2 C1 (Addgene, plasmid nr 54563) by seamless PCR cloning. The linker between Cherry2 and amisyn translates into the peptide SGLRSRAQASNSAV. The plasmid N1 NPY-EGFP-mCherry coding for NPY-linker(TVPRARDPPVAT)-EGFP-linker(KRSGGSGGSGGS)-mCherry was made by seamless PCR cloning. The correct open reading frame of both Cherry2-linker-amisyn and NPY-EGFP-mCherry was confirmed by Sanger sequencing (Eurofins, Germany). The NPY-tdOrange2 adeno virus was made using the RAPAd vector system (Cell Biolabs, San Diego, USA). NPY-tdOrange2 [87] was cloned into the pacAd5 CMVK-NpA Shuttle plasmid (Cell Biolabs). Virus was produced in HEK293 cells and isolated according to the instructions of the manufacturer (Cell Biolabs).

Solutions

Cells were imaged in (mM) 138 NaCl, 5.6 KCl, 1.2 $MgCl_2$, 2.6 $CaCl_2$, 10 D-glucose 5 HEPES (pH 7.4 with NaOH) at 32-34 °C. Exocytosis was evoked with high 75 mM K^+ (equimolarly replacing Na^+), applied by computer-timed local pressure ejection through a pulled glass capillary. For K^+-induced exocytosis, spontaneous depolarizations were prevented with 200 µM diazoxide (50 µM for Fig 5e-h). In Fig 5e-h, exocytosis was evoked by sulfonylureas (500 µM tolbutamide, 200 µM glibenclamide or 200 µM gliclizide). For electrophysiology, glucose was reduced to 3 mM, and the electrodes were filled with (mM) 125 CsCl, 10 NaCl, 1.2 $MgCl_2$, 5 EGTA, 4 $CaCl_2$, 3 Mg-ATP, 0.1 cAMP, 10 HEPES (pH 7.15 using CsOH).

Immunocytochemistry

To quantify the overexpression, INS-1 cell were transfected with either Cherry2-amisyn or Dynamin1-GFP, fixed 24h later in 3.8% formaldehyde in phosphate-buffered saline (PBS) for 30 min at 25 °C and washed in PBS. The cells were permeabilized in 0.2% Triton X-100 in PBS for 5 min and washed in PBS. Blocking was done using 5% FBS in PBS for 1-2 h at 25 °C. Cells were then incubated with a primary antibody (anti-Dynamin1,

ab52852 abcam or anti-Amisyn, ab153974 abcam) both diluted 1/50 in 5% FCS in PBS over night at 4°C and washed again in PBS. Incubation with secondary antibody (Alexa Fluor 488 anti-rabbit or Alexa Fluor 555 anti-rabbit, Invitrogen) diluted 1/1000 in 5% FCS in PBS was performed for 1 h at 25 °C and subsequently the cells were washed in PBS.

TIRF microscopy

Human cells were imaged using a lens-type total internal reflection (TIRF) microscope, based on an AxioObserver Z1 with a 100x/1.45 objective (Carl Zeiss). TIRF illumination with a calculated decay constant of ~100 nm was created using two DPSS lasers at 491 and 561 nm (Cobolt, Stockholm, Sweden) that passed through a cleanup filter (zet405/488/561/640x, Chroma) and was controlled with an acousto-optical tunable filter (AA-Opto, France). Excitation and emission light were separated using a beamsplitter (ZT405/488/561/640rpc, Chroma) and the emission light chromatically separated (QuadView, Roper) onto separate areas of an EMCCD camera (QuantEM 512SC, Roper) with a cutoff at 565 nm (565dcxr, Chroma) and emission filters (ET525/50m and 600/50m, Chroma). Scaling was 160 nm per pixel.

INS1 and mouse cells were imaged using a custom-built lens-type TIRF microscope based on an AxioObserver D1 microscope and a 100x/1.45 NA objective (Carl Zeiss). Excitation was from two DPSS lasers at 473 nm and 561 nm (Cobolt), controlled with an acousto-optical tunable filter (AOTF, AA-Opto) and using dichroic Di01-R488/561 (Semrock). The emission light was separated onto the two halves of a 16-bit EMCCD camera (Roper Cascade 512B, gain setting at 3,800 a.u. throughout) using an image splitter (DualView, Photometrics) with ET525/50m and 600/50m emission filters (Chroma). Scaling was 100 nm per pixel for INS-1 experiments and 160 nm for mouse cells. The frame rate was 10 frames*s^{-1}, with 100 ms exposures.

Image analysis

Exocytosis events were identified manually based on the characteristic rapid loss of the granule marker fluorescence (most fluorescence lost within 1-2 frames) in cells which exhibited minimum of 1 event/cell (except mouse cells, where all cells were included). Events were classified as flash events if they exhibited an increase in the fluorescence signal before the rapid loss of the granule fluorescence. The NPY release times were obtained for both types of events by non-linear fitting with a discontinuous function in Origin as described previously [87]. Protein binding to the release site ($\Delta F/S$) was measured as described previously [43].

357

358 **Electrophysiology**

359 ATP release was measured in INS1 cells expressing RFP-tagged $P2X_2$ receptor [4]. Cells were voltage-clamped
360 in whole-cell mode using an EPC-9 amplifier and PatchMaster software (Heka Elektronik, Lambrecht, Germany)
361 with patch-clamp electrodes pulled from borosilicate glass capillaries that were coated with Sylgard close to
362 the tips, and fire-polished (resistance 2-4 MΩ). The free $[Ca^{2+}]$ was calculated to be 600 nM (WEBMAXC
363 standard) and elicited exocytosis that was detected as $P2X_2$-dependent inward current spikes. Currents were
364 filtered at 1 kHz and sampled at 5 kHz. Spike analysis was performed using automated program for
365 amperometric recordings in IGOR Pro [89], with the threshold set at eight times the RMS noise during event-free
366 section of recording.

367

368 **Statistics**

369 Data are presented as mean ± SEM unless otherwise stated. Statistical significance was tested (unless
370 otherwise stated) and is indicated by asterisks (*$p < 0.05$, **$p < 0.01$, ***$p < 0.001$). The not normally
371 distributed exocytosis rates and ratios of flash events were tested with Kruskal Wallis with post hoc Dunn test
372 and NPY release times were tested with Kolmogorov-Smirnov test.

373

374 **Acknowledgement**

375 We thank J. Saras, P.-E. Lund, and A. Thonig (Uppsala University) for expert technical assistance, and D.
376 Machado (University of La Laguna) for spike analysis software. The work was supported by the Swedish
377 Research Council (2014-02575, 2017-00956, 2018-02871), Diabetes Wellness Network Sweden, Swedish
378 Diabetes Foundation, European Foundation for the Study of Diabetes (EFSD-MSD), Swedish Society for Medical
379 Research, Hjärnfonden, and the NovoNordisk and Family Ernfors foundations. A.G. was supported by N.R.G.
380 was supported by the European Foundation for the Study of Diabetes (EFSD) Rising Star Research Fellowship,
381 the Swedish Society for Medical Research (SSMF) and the Novo Nordisk Foundation. S.D. was supported by
382 grants from the Norwegian Research Council (NFR) and Helse-Bergen. Human islets for research were provided
383 by the Nordic Network for Islet Transplantation (supported by JDRF grant 31-2008-416, ECIT Islet for Basic
384 Research Program).

Declaration of Interests

The authors declare no competing interests.

References

1. Albillos, A. *et al.* The exocytotic event in chromaffin cells revealed by patch amperometry. *Nature* **389,** 509–512 (1997).

2. Bao, H. *et al.* Exocytotic fusion pores are composed of both lipids and proteins. *Nat Struct Mol Biol* **23,** 67–73 (2016).

3. Sharma, S. & Lindau, M. The fusion pore, 60 years after the first cartoon. *FEBS Lett.* (2018). doi:10.1002/1873-3468.13160

4. Obermüller, S. *et al.* Selective nucleotide-release from dense-core granules in insulin-secreting cells. *J Cell Sci* **118,** 4271–4282 (2005).

5. Barg, S. *et al.* Delay between fusion pore opening and peptide release from large dense-core vesicles in neuroendocrine cells. *Neuron* **33,** 287–299 (2002).

6. MacDonald, P. E. E., Braun, M., Galvanovskis, J. & Rorsman, P. Release of small transmitters through kiss-and-run fusion pores in rat pancreatic beta cells. *Cell Metab* **4,** 283–290 (2006).

7. Alvarez de Toledo, G., Fernández-Chacón, R., Fernández, J. M., Fernandez-Chacon, R. & Fernandez, J. M. Release of secretory products during transient vesicle fusion. *Nature* **363,** 554–558 (1993).

8. Hanna, S. T. *et al.* Kiss-and-run exocytosis and fusion pores of secretory vesicles in human beta-cells. *Pflügers Arch. Eur. J. Physiol.* **457,** 1343–50 (2009).

9. Breckenridge, L. J. & Almers, W. Currents through the fusion pore that forms during exocytosis of a secretory vesicle. *Nature* **328,** 814–7 (1987).

10. Lollike, K., Borregaard, N. & Lindau, M. The exocytotic fusion pore of small granules has a conductance similar to an ion channel. *J Cell Biol* **129,** 99–104 (1995).

11. Anantharam, A., Onoa, B., Edwards, R. H., Holz, R. W. & Axelrod, D. Localized topological changes of the plasma membrane upon exocytosis visualized by polarized TIRFM. *J. Cell Biol.* **188,** 415–428 (2010).

12. Taraska, J. W., Perrais, D., Ohara-Imaizumi, M., Nagamatsu, S. & Almers, W. Secretory granules are recaptured largely intact after stimulated exocytosis in cultured endocrine cells. *Proc. Natl. Acad. Sci. U. S. A.* **100,** 2070–2075 (2003).

13. Tsuboi, T. & Rutter, G. A. Insulin secretion by 'kiss-and-run' exocytosis in clonal pancreatic islet beta-cells.

Biochem. Soc. Trans. **31,** 833–836 (2003).

14. Shin, W. *et al.* Visualization of Membrane Pore in Live Cells Reveals a Dynamic-Pore Theory Governing Fusion and Endocytosis. *Cell* **173,** 934–945.e12 (2018).

15. Hellman, B., Dansk, H. & Grapengiesser, E. Pancreatic beta-cells communicate via intermittent release of ATP. *Am. J. Physiol. Endocrinol. Metab.* **286,** E759–E765 (2004).

16. Salehi, A. *et al.* Inhibition of purinoceptors amplifies glucose-stimulated insulin release with removal of its pulsatility. *Diabetes* **54,** 2126–2131 (2005).

17. Poulsen, C. R. *et al.* Multiple sites of purinergic control of insulin secretion in mouse pancreatic beta-cells. *Diabetes* **48,** 2171–2181 (1999).

18. Richards-Williams, C., Contreras, J. L., Berecek, K. H. & Schwiebert, E. M. Extracellular ATP and zinc are co-secreted with insulin and activate multiple P2X purinergic receptor channels expressed by islet beta-cells to potentiate insulin secretion. *Purinergic Signal.* **4,** 393–405 (2008).

19. Tuduri, E., Filiputti, E., Carneiro, E. M. & Quesada, I. Inhibition of Ca2+ signaling and glucagon secretion in mouse pancreatic ?-cells by extracellular ATP and purinergic receptors. *AJP Endocrinol. Metab.* **294,** E952–E960 (2008).

20. Weitz, J. R. *et al.* Mouse pancreatic islet macrophages use locally released ATP to monitor beta cell activity. *Diabetologia* **61,** 1–11 (2017).

21. Jin, Y., Korol, S. V., Jin, Z., Barg, S. & Birnir, B. In Intact Islets Interstitial GABA Activates GABAA Receptors That Generate Tonic Currents in α-Cells. *PLoS One* **8,** (2013).

22. Ben-Othman, N. *et al.* Long-Term GABA Administration Induces Alpha Cell-Mediated Beta-like Cell Neogenesis. *Cell* **168,** 73–85.e11 (2017).

23. Cabrera, O. *et al.* Glutamate is a positive autocrine signal for glucagon release. *Cell Metab.* **7,** 545–54 (2008).

24. Alés, E. *et al.* High calcium concentrations shift the mode of exocytosis to the kiss-and-run mechanism. *Nat. Cell Biol.* **1,** 40–44 (1999).

25. Calejo, A. I. *et al.* cAMP-mediated stabilization of fusion pores in cultured rat pituitary lactotrophs. *J Neurosci* **33,** 8068–8078 (2013).

26. Scepek, S., Coorssen, J. R. & Lindau, M. Fusion pore expansion in horse eosinophils is modulated by Ca2+ and protein kinase C via distinct mechanisms. *EMBO J.* **17,** 4340–4345 (1998).

27. Chiang, H.-C. *et al.* Post-fusion structural changes and their roles in exocytosis and endocytosis of dense-core vesicles. *Nat. Commun.* **5,** 3356 (2014).

28. Jackson, J. *et al.* Small molecules demonstrate the role of dynamin as a bi-directional regulator of the exocytosis fusion pore and vesicle release. *Mol. Psychiatry* **20,** 810–9 (2015).

29. Tsuboi, T., McMahon, H. T. & Rutter, G. A. Mechanisms of dense core vesicle recapture following 'kiss and run' ('cavicapture') exocytosis in insulin-secreting cells. *J. Biol. Chem.* **279,** 47115–24 (2004).

30. Graham, M. E., O'Callaghan, D. W., McMahon, H. T. & Burgoyne, R. D. Dynamin-dependent and dynamin-independent processes contribute to the regulation of single vesicle release kinetics and quantal size. *Proc. Natl. Acad. Sci. U. S. A.* **99,** 7124–7129 (2002).

31. Artalejo, C. R., Henley, J. R., McNiven, M. A. & Palfrey, H. C. Rapid endocytosis coupled to exocytosis in adrenal chromaffin cells involves Ca2+, GTP, and dynamin but not clathrin. *Proc. Natl. Acad. Sci. U. S. A.* **92,** 8328–8332 (1995).

32. Aoki, R. *et al.* Duration of fusion pore opening and the amount of hormone released are regulated by myosin II during kiss-and-run exocytosis. *Biochem J* **429,** 497–504 (2010).

33. Wen, P. J. *et al.* Actin dynamics provides membrane tension to merge fusing vesicles into the plasma membrane. *Nat. Commun.* **7,** 12604 (2016).

34. Collins, S. C. *et al.* Increased expression of the diabetes gene SOX4 reduces insulin secretion by impaired fusion pore expansion. *Diabetes* **65,** 1952–1961 (2016).

35. Logan, T., Bendor, J., Toupin, C., Thorn, K. & Edwards, R. H. α-Synuclein promotes dilation of the exocytotic fusion pore. *Nat. Neurosci.* **20,** 681–689 (2017).

36. Henquin, J. C. Triggering and amplifying pathways of regulation of insulin secretion by glucose. *Diabetes* **49,** 1751–1760 (2000).

37. Kawasaki, H. *et al.* A Family of cAMP-Binding Proteins That Directly Activate Rap1. *Science (80-.).* **282,** 2275–2279 (1998).

38. Ozaki, N. *et al.* cAMP-GEFII is a direct target of cAMP in regulated exocytosis. *Nat. Cell Biol.* **2,** 805–811 (2000).

39. Alenkvist, I., Gandasi, N. R. N. R., Barg, S. & Tengholm, A. Recruitment of Epac2A to insulin granule docking sites regulates priming for exocytosis. *Diabetes* **66,** 2610–2622 (2017).

40. Zhang, C. L. C.-L. *et al.* The cAMP sensor Epac2 is a direct target of antidiabetic sulfonylurea drugs. *Science (80-.).* **325,** 607–10 (2009).

41. Huang, X. *et al.* Fast, long-term, super-resolution imaging with Hessian structured illumination microscopy. *Nat. Biotechnol.* **36,** 451–459 (2018).

42. Ferraro, F., Eipper, B. A. & Mains, R. E. Retrieval and reuse of pituitary secretory granule proteins. *J. Biol. Chem.* **280,** 25424–25435 (2005).

43. Gandasi, N. R. & Barg, S. Contact-induced clustering of syntaxin and munc18 docks secretory granules at the exocytosis site. *Nat Commun* **5,** 3914 (2014).

44. Schwede, F. *et al.* Structure-Guided Design of Selective Epac1 and Epac2 Agonists. *PLoS Biol.* **13,** (2015).

45. Gjertsen, B. T. *et al.* Novel (Rp)-cAMPS analogs as tools for inhibition of cAMP-kinase in cell culture. Basal cAMP-kinase activity modulates interleukin-1 beta action. *J. Biol. Chem.* **270,** 20599–607 (1995).

46. Zhu, Y. *et al.* Biochemical and Pharmacological Characterizations of ESI-09 Based EPAC Inhibitors: Defining the ESI-09 'Therapeutic Window'. *Sci. Rep.* **5,** 9344 (2015).

47. Kopperud, R. K. *et al.* Increased microvascular permeability in mice lacking Epac1 (Rapgef3). *Acta Physiol.* **219,** 441–452 (2017).

48. Dyachok, O. *et al.* Glucose-induced cyclic AMP oscillations regulate pulsatile insulin secretion. *Cell Metab.* **8,** 26–37 (2008).

49. Barg, S. *et al.* The stimulatory action of tolbutamide on Ca2+-dependent exocytosis in pancreatic b-cells is mediated by a 65-kDa mdr-like P-glycoprotein. *Proc. Natl. Acad. Sci.* **96,** 5539–5544 (1999).

50. Machado, J. D., Morales, A., Gomez, J. F. & Borges, R. cAmp modulates exocytotic kinetics and increases quantal size in chromaffin cells. *Mol. Pharmacol.* **60,** 514–20 (2001).

51. Hatakeyama, H., Kishimoto, T., Nemoto, T., Kasai, H. & Takahashi, N. Rapid glucose sensing by protein kinase A for insulin exocytosis in mouse pancreatic islets. *J. Physiol.* **570,** 271–82 (2006).

52. Leclerc, I. *et al.* Metformin, but not leptin, regulates AMP-activated protein kinase in pancreatic islets: impact on glucose-stimulated insulin secretion. *Am. J. Physiol. Endocrinol. Metab.* **286,** E1023-31 (2004).

53. Eliasson, L. *et al.* SUR1 regulates PKA-independent cAMP-induced granule priming in mouse pancreatic b-cells. *J. Gen. Physiol.* **121,** 181–197 (2003).

54. Takahashi, T. *et al.* Antidiabetic sulfonylureas and cAMP cooperatively activate Epac2A. *Sci. Signal.* **6,** ra94 (2013).

55. Herbst, K. J. J., Coltharp, C., Amzel, L. M. M. & Zhang, J. Direct Activation of Epac by Sulfonylurea Is Isoform Selective. *Chem. Biol.* **18,** (2011).

56. Abdulreda, M. H., Rodriguez-Diaz, R., Caicedo, A. & Berggren, P.-O. Liraglutide Compromises Pancreatic β Cell Function in a Humanized Mouse Model. *Cell Metab.* **23,** 541–6 (2016).

57. Yabe, D. & Seino, Y. Dipeptidyl peptidase-4 inhibitors and sulfonylureas for type 2 diabetes: Friend or foe? *Journal of Diabetes Investigation* **5,** 475–477 (2014).

58. Takahashi, H. *et al.* Role of Epac2A/Rap1 signaling in interplay between incretin and sulfonylurea in insulin secretion. *Diabetes* **64,** 1262–72 (2015).

59. Seino, S., Takahashi, H., Fujimoto, W. & Shibasaki, T. Roles of cAMP signalling in insulin granule exocytosis. *Diabetes. Obes. Metab.* **11 Suppl 4,** 180–188 (2009).

60. Fujimoto, K. *et al.* Piccolo, a Ca2+ Sensor in Pancreatic beta -Cells. Involvment of cAMP-GEFII·Rim2·Piccolo complex in cAMP-dependent exocytosis. *J. Biol. Chem.* **277,** 50497–50502 (2002).

61. Shibasaki, T. *et al.* Essential role of Epac2/Rap1 signaling in regulation of insulin granule dynamics by cAMP. *Proc. Natl. Acad. Sci. U. S. A.* **104,** 19333–19338 (2007).

62. Dzhura, I. *et al.* Phospholipase C-ε links Epac2 activation to the potentiation of glucose-stimulated insulin secretion from mouse islets of Langerhans. *Islets* **3,** 121–128 (2011).

63. Marte, B. M., Rodriguez-Viciana, P., Wennström, S., Warne, P. H. & Downward, J. R-Ras can activate the phosphoinositide 3-kinase but not the MAP kinase arm of the Ras effector pathways. *Curr. Biol.* **7,** 63–71 (1997).

64. Kang, L. *et al.* Munc13-1 is required for the sustained release of insulin from pancreatic beta cells. *Cell Metab.* **3,** 463–468 (2006).

65. Ramachandran, R. & Schmid, S. L. Real-time detection reveals that effectors couple dynamin's GTP-dependent conformational changes to the membrane. *EMBO J.* **27,** 27–37 (2008).

66. Abbineni, P. S., Axelrod, D. & Holz, R. W. Visualization of expanding fusion pores in secretory cells. *J. Gen. Physiol.* **150,** 1640–1646 (2018).

67. Marks, B. *et al.* GTPase activity of dynamin and resulting conformation change are essential for endocytosis. *Nature* **410,** 231–235 (2001).

68. Trexler, A. J., Sochacki, K. A. & Taraska, J. W. Imaging the recruitment and loss of proteins and lipids at single sites of calcium-triggered exocytosis. *Mol. Biol. Cell* **27,** 2423–34 (2016).

69. Perrais, D., Kleppe, I. C. C., Taraska, J. W. W. & Almers, W. Recapture after exocytosis causes differential retention of protein in granules of bovine chromaffin cells. *J Physiol* **560,** 413–428 (2004).

70. Taraska, J. W. & Almers, W. Bilayers merge even when exocytosis is transient. *Proc. Natl. Acad. Sci. U. S. A.* **101,** 8780–8785 (2004).

71. Zhao, W.-D. *et al.* Hemi-fused structure mediates and controls fusion and fission in live cells. *Nature* **534,** 548–552 (2016).

72. Anantharam, A. *et al.* A new role for the dynamin GTPase in the regulation of fusion pore expansion. *Mol. Biol. Cell* **22,** 1907–18 (2011).

73. Wang, C. T. *et al.* Synaptotagmin modulation of fusion pore kinetics in regulated exocytosis of dense-core vesicles. *Science (80-.).* **294,** 1111–1115 (2001).

74. Wu, Z. *et al.* Dilation of fusion pores by crowding of SNARE proteins. *Elife* **6,** e22964 (2017).

75. Braun, M., Ramracheya, R. & Rorsman, P. Autocrine regulation of insulin secretion. *Diabetes, Obesity and Metabolism* **14,** 143–151 (2012).

76. Caicedo, A. Paracrine and autocrine interactions in the human islet: More than meets the eye. *Seminars in Cell and Developmental Biology* **24,** 11–21 (2013).

77. Leibiger, I. B., Leibiger, B. & Berggren, P.-O. Insulin Signaling in the Pancreatic β-Cell. *Annu. Rev. Nutr.* **28,** 233–251 (2008).

78. Vergari, E. *et al.* Insulin inhibits glucagon release by SGLT2-induced stimulation of somatostatin secretion. *Nat. Commun.* **10,** 139 (2019).

79. Ravier, M. A. & Rutter, G. A. Glucose or insulin, but not zinc ions, inhibit glucagon secretion from mouse pancreatic alpha-cells. *Diabetes* **54,** 1789–97 (2005).

80. Rorsman, P. *et al.* Glucose-inhibition of glucagon secretion involves activation of GABAA-receptor chloride channels. *Nature* **341,** 233–236 (1989).

81. Soltani, N. *et al.* GABA exerts protective and regenerative effects on islet beta cells and reverses diabetes. *Proc. Natl. Acad. Sci.* **108,** 11692–11697 (2011).

549 82. Khan, S. *et al.* Autocrine activation of P2Y1 receptors couples Ca2+ influx to Ca2+ release in human pancreatic beta
550 cells. *Diabetologia* **57,** 2535–2545 (2014).

551 83. Jacques-Silva, M. C. *et al.* ATP-gated P2X3 receptors constitute a positive autocrine signal for insulin release in the
552 human pancreatic cell. *Proc. Natl. Acad. Sci.* **107,** 6465–6470 (2010).

553 84. Bertrand, G., Gross, R., Ribes, G. & Loubatières-Mariani, M. M. P2 purinoceptor agonists stimulate somatostatin
554 secretion from dog pancreas. *Eur. J. Pharmacol.* **182,** 369–373 (1990).

555 85. Hohmeier, H. E. *et al.* Isolation of INS-1-derived cell lines with robust ATP-sensitive K+ channel-dependent and -
556 independent glucose-stimulated insulin secretion. *Diabetes* **49,** 424–430 (2000).

557 86. Idevall-Hagren, O., Jakobsson, I., Xu, Y. & Tengholm, A. Spatial Control of Epac2 Activity by cAMP and Ca2+-
558 Mediated Activation of Ras in Pancreatic Cells. *Sci. Signal.* **6,** ra29-ra29 (2013).

559 87. Gandasi, N. R. *et al.* Survey of Red Fluorescence Proteins as Markers for Secretory Granule Exocytosis. *PLoS One*
560 **10,** e0127801 (2015).

561 88. Goto, M. *et al.* Refinement of the automated method for human islet isolation and presentation of a closed
562 system for in vitro islet culture. *Transplantation* **78,** 1367–75 (2004).

563 89. Segura, F., Brioso, M. A., Gómez, J. F., Machado, J. D. & Borges, R. Automatic analysis for amperometrical
564 recordings of exocytosis. *J. Neurosci. Methods* **103,** 151–156 (2000).

565

Figure legends

Figure 1: cAMP-dependent fusion pore restriction depends on Epac (but not PKA).

(a) Examples of single granule exocytosis in human β-cells expressing NPY-Venus and challenged with 75 mM K^+. Full fusion (left) and flash event (right), where sudden loss of the granule label was preceded by a transient fluorescence increase. Arrows indicate moment of fusion pore opening (orange) and content release (blue).

(b) Cartoons illustrating the interpretation of events in a.

(c) Fluorescence time courses for the events in b. Overlaid (green) are fitted functions used to estimate NPY release time.

(d) Fraction of flash events in experiments as in a-c, in cells exposed to the indicated agents; forskolin (fsk, P=0.01 vs ctrl), exendin-4 (Ex4, P=0.02 vs ctrl), ESI-09 ($P=3*10^{-4}$ vs fsk), S223 (P=0.04 vs ctrl), fsk+S223 (P=0.99 vs fsk), RP-8 (P=0.91 vs fsk) and Rp-8 + S223 (P=0.19 vs ctrl; Kruskal Wallis/Dunn). Number of donors analyzed: 7 (CTR); 5 (fsk); 4 (Ex4); 7 (fsk+ESI09); 6 (S223); 6 (fsk+S223); 7 (RP-8); 4 (Rp-8+S223). n, number of cells.

(e) Cumulative frequency histograms of NPY release times; fsk ($P=9*10^{-7}$ vs ctrl), Ex4 ($P=1*10^{-6}$ vs ctrl), S223 ($P=4*10^{-6}$ vs ctrl), ESI-09 ($P=2*10^{-4}$ vs fsk), Fsk+S223 (n.s. vs fsk), RP-8 (n.s. vs fsk) and RP-8+S223 (P=0.016 vs ctrl); Kolmogorov-Smirnov test). Inset shows median NPY release times for 170 (CTR), 197 (fsk), 155 (Ex4), 81 (ESI-09), 240 (S223), 328 (fsk+S223), 277 (RP-8) and 227 (Rp-8+S223) events.

(f) Exocytosis during 40 s of K^+-stimulation for control (CTR) and with forskolin (fsk, 2 µM, P=0.002 vs ctrl; Kruskal Wallis/Dunn) or Exendin-4 (Ex4, 10 nM, P=0.005 vs ctrl) or S223 (5µM, P=0.002 vs ctrl) or RP-8+S223 (P=0.012 vs ctrl and n.s. vs S223) in the bath solution. Inhibitors of Epac (ESI-09, 10 µM, $P=9*10^{-}7$ vs fsk) or PKA (RP-8, 100 µM, n.s. vs fsk) or Epac2 activator S223 (n.s. vs fsk), one-way ANOVA with Games-Howell post hoc test) were supplied in addition to forskolin. Flash exocytosis (in color) and full fusions (in white) are shown separately. n, number of cells.

Figure 2: Epac2 overexpression prolongs NPY release times.

(a) Cumulative exocytosis in INS-1 cells stimulated with 75 mM K^+; grey for control cells, purple for cells expressing Epac2-EGFP (both also expressed NPY-tdmOrange2); fsk indicates forskolin in the bath solution. CTR, n=13 (4 preps); Epac2, n=11 (2 preps); CTR+fsk, n=15 (5 preps); Epac2+fsk, n=14 cells (2 preps).

(b) Total exocytosis in (a), separated into flash events (color) and full fusion (white). Epac2 expression reduced full fusion events (no fsk P=0.06; with fsk P=0.01, Kruskal Wallis/Dunn). n, number of cells.

(c) Fraction of flash events in (a-b). (Kruskal Wallis/Dunn). n, number of cells.

(d) NPY release times for conditions in a-c. Epac overexpression increased NPY release times in absence (P=0.014) but not in presence of fsk (P=0.87, Kolmogorov-Smirnov test). Inset shows the NPY release times for 38 (CTR), 27 (Epac2), 119 (CTR+fsk) and 77 (Epac2+fsk) events.

Figure 3: Cytosolic cAMP slows ATP release by activating Epac.

(a) Electrophysiological detection of nucleotide release events in INS-1 cells expressing $P2X_2$-RFP. Cartoon of the assay (left) and example current spike (black) with fit and analysis parameters (red; T_{half}, tau and slope during 25% to 75% of peak).

(b) Representative $P2X_2$ currents for control (black), and with cAMP (green) or with cAMP together with ESI-09 (purple) in the electrode solution.

(c) Spike frequency conditions in (b). n of events (on top) and n of cells (on bars); 2 preps for each condition.

(d-f) Cumulative frequency histograms of spike half width (d), decay constant tau (e), and slope of the rising phase (25% and 75% of peak, (f)) for CTR (n=410 spikes, 14 cells), +cAMP (n=1240, 14 cells) and +ESI-09+cAMP (n=552, 15 cells) with medians in the insets. cAMP increased half-width ($P=4.1*10^{-31}$ vs ctrl, Kolmogorov-Smirnov test), tau ($P=2.7*10^{-32}$, Kolmogorov-Smirnov test), and rising slope ($P=4.7*10^{-19}$, Kolmogorov-Smirnov test); the effects were reversed by ESI-09 ($P=3.4*10^{-21}$, $P=3.6*10^{-22}$, and $P=1.3*10^{-9}$, Kolmogorov-Smirnov test), respectively.

Figure 4: Fusion pores expand rapidly in Epac2$^{-/-}$ (*Rapgef4*$^{-/-}$) mice.

(a-b) Examples of NPY-tdmOrange2 exocytosis events in β-cells from Epac2$^{-/-}$ mice or from wildtype littermates, stimulated with 75 mM K^+ in presence of forskolin. Note absence of a flash in Epac2 ko.

(c) Fraction of flash events for experiments in (a-b); differences are significant in absence (P=0.027, Kruskal Wallis/Dunn test) or presence of fsk (P=0.011). Number of mice: 4 (WT); 4 (Epac2 KO); 5 (WT+fsk); 2 (Epac2 KO+fsk). n, number of cells.

(d) Cumulative exocytosis for experiments in absence of forskolin (a,c left) for wildtype (black) and Epac2$^{-/-}$ cells (red), differences are n.s.

(e) Cumulative exocytosis for experiments in presence of forskolin (b,c right) for wildtype (black) and Epac2$^{-/-}$ cells (red). P=0.003, Kruskal Wallis/Dunn test.

(f-g) Cumulative frequency histograms and medians (inset) of NPY release times for exocytotic events in d (no forskolin, 23 events for wt, 22 for Epac2$^{-/-}$) and E (with forskolin, 50 events for wt, 9 for Epac2-/-). Differences in f are significant (P=0.043; Kolmogorov-Smirnov test).

Figure 5: Sulfonylureas cause fusion pore restriction.

(a) Cartoon of the experimental design in (b-d). INS-1 cells expressing NPY-tdmOrange2 were bathed in 10 mM glucose, diazoxide (200 µM) and either 200 µM tolbutamide (tolb), 50 µM glibenclamide (glib) or 50 µM gliclizide (gliz); exocytosis was evoked by acute exposure to 75 mM K^+.

(b) Exocytosis in absence (left) or presence (right) of fsk (2 µM) for flash events (color) and full fusions (white). Total exocytosis was increased by sulfonylurea in absence of fsk (P=0.15 tolb; P=0.05 glib, P=0.005 gliz, Kruskal Wallis/Dunn test vs ctrl/no fsk), but not in its presence (P=0.23 tolb; P=0.16 glib, P=0.10 glic). Sulfonylurea reduced full fusion events in presence of fsk (P=0.0045 tolb, P=0.00032 glib, 0.022 gliz, t-test). n of preps: 4 (CTR); 3 (tolb); 2 (glib); 3 (gliz); 5 (CTR+fsk); 3 (tolb+fsk); 3 (glib+fsk); 2 (gliz+fsk). n, number of cells.

(c) Fraction of flash events for experiments in (b); Kruskal-Wallis/Dunn Test against ctrl/no fsk: P=0.015 tolb, P=0.001 glib, P=0.097 gliz, and against control+fsk: P=0.07 tolb; P=0.002 glib; P=0.14 gliz;); n, number of cells.

(d) Cumulative frequency histograms and medians (insets) of NPY release times for (b-c). Differences vs control are significant in the absence of fsk: P=9.1*10^{-4} tolb, P=0.003 glib, P=0.015 gliz, Kolmogorov-Smirnov test). Insets show NPY release times for 38 (CTR), 74 (tolb), 79 (glib), 95 (gliz) events and inset on the right for 111 (CTR), 104 (tolb), 127 (glib) and 54 (gliz) events in presence of fsk.

(e) Cartoon of the experimental design in (f-h). Cells were bathed in 10 mM glucose, 2 µM fsk, 50 µM diazoxide and acutely exposed to sulfonylureas (500 µM tolb, 100 µM glib or 100 µM gliz) during the recording period.

(f) Exocytosis in presence of fsk (2 µM) for flash events (color) and full fusions (white). Differences are not significant (P=0.16 Kruskal Wallis test). n, number of cells.

(g) Fraction of flash events for experiments in (f). Differences are not significant (P=0.98 Kruskal Wallis test).

(h) Cumulative frequency histograms and medians (inset) of NPY release times for (f-g). Inset shows NPY release times for 111 (CTR), 68 (tolb), 34 (glib) and 31 (gliz) events.

Figure 6: Fusion pore regulation by dynamin1 and amisyn is cAMP-dependent.

(a-b) Example image sequence of transient recruitment of dynamin1-GFP (a, lower) or mCherry-amisyn (b, lower) to granules (upper, labeled with NPY-tdmOrange2 or NPY-EGFP) during K^+-stimulated exocytosis in presence of forskolin.

(c) Average time course (±SEM) of dynamin1-GFP (dyn) fluorescence during 34 flash-type exocytosis events (red) and 8 full-fusion type events (black) in presence of forskolin; and 9 flash events in presence of fsk+ESI09 (blue); data points represent average of 5 frames and time is relative to the flash onset in the granule signal.

(d) Cumulative frequency histograms and medians (inset, with p for Kolmogorov-Smirnov test) of NPY release times in presence of fsk in cells expressing dynamin1-EGFP (red), dynamin with added ESI09 (blue) or control (black). 119 (CTR), 42 (dyn), 24 (dyn+ESI09) events. n of preps: 5 (C+fsk); 1 (dyn); 2 (dyn+ESI-09).

(e) Fraction of flash events in (d). n, number of cells, p for Kruskal-Wallis/Dunns test.

(f) Average time course (±SEM) of mCherry-amisyn (amis) fluorescence (red n=274 flash events; black n=46 full fusion events) or in presence of fsk+ESI09 (blue; n=56 flash events).

(g) Cumulative frequency histograms and medians (inset, with Kolmogorov-Smirnov test) of NPY release times in cells expressing mCherry-amisyn, amysin with ESI09, or control; fsk was present. 213 (CTR), 320 (amisyn), and 90 (amis+ESI09) events. n of preps: 2 for each.

(h) Fraction of flash events in (g); p for Kruskal-Wallis/Dunn test. n, number of cells.

(i) As in c, but without forskolin for control (black), dynamin (red), and dynamin with S223 (green); n=37 flash events, n=39 full fusion events for dyn and n=40 flash events for dyn+S223.

(j-k) As in (d-e), but for 38 (ctrl, black), 76 (dynamin1, red) and 55 (Dyn+S223, green) events in the absence of forskolin. n of preps: 4 (C-fsk); 2 (dyn); 2 (dyn+S223).

(l) As in f, but without forskolin present; 65 flash events (red) and 73 full fusion events (black) for amisyn, and 154 flash events for amisyn + S223 (green).

(m-n) As in (g-h), but for 123 (ctrl, black), 138 (amisyn, red) and 174 (amis+S223, green) events in the absence of forskolin. n of preps: 1 (C-fsk); 2 (amis); 2 (amis+S223).

Figure 7: Summary of fusion pore characteristics.

Fraction of events with restricted fusion pores, NPY release time and exocytosis rate for Epac2 KO (first column), controls (second column) and with Epac2 overexpression (third column) in absence (upper rows) and

presence of tolbutamide (bottom rows). Changes in exocytosis are compared to controls without (left half columns) or with (right half columns) forskolin. See Figure 7-source data 1 for details.

Supplemental figure legends

Figure 1 – Figure supplement 1: cAMP increases NPY release times in INS1 cells.

(a-b) K^+ stimulated exocytosis of NPY-tdmOrange2 granules in INS1 cells is significantly increased in presence of (A) forskolin (fsk; 2 µM; P=0.002) or (B) exendin-4 (Ex4; 10 nM; P=0.03). CTR, n= 13 cells; Fsk, n=15; Ex4, n=16. n of preps: 4 (CTR); 5 (+fsk); 2 (+Ex4).

(c) Total exocytosis in (A-B) separated for events with flashes (in color) and full fusion events (in white); significance (t-test) is given for flash events.

(d) Cumulative frequency histograms of NPY release times in (A-B); note longer NPY release times in presence of fsk (P=0.011) or Ex4 (P=0.018, Kolmogorov-Smirnov test). Inset plots the median NPY release times for 38 (CTR), 119 (fsk) and 111 (Ex4) events.

(e) Percentage of flash events (P=0.23 for fsk, P=0.14 for Ex4 vs. control, u-test). n, number of cells.

Figure 5 – Figure supplement 1: Granule pH is unchanged by forskolin or tolbutamide and does not affect pore lifetime.

(a) Image sequences of a single NPY-EGFP-mCherry granule in an INS1 cells, exposed to 10 mM NH_4^+ (arrow); the green (top) and red color channels (bottom) of this ratiometric pH-probe are shown.

(b) Green/red fluorescence ratio as measure of granule pH in controls (black), presence of fsk (green), tolbutamide (tlb, cyan), or both (blue); none of the values is significantly different from control; n, number of cells (20 granules each).

(c) The fluorescence ratio for the same granules as in (b), after alkalization with 10 mM NH_4^+ was similar with fsk (P=0.06), tlb (P=0.06) or tlb+fsk (P=0.91).

(d) K^+-stimulated exocytosis of a single NPY-EGFP-mCherry granule; green (top) and red fluorescence (bottom) are shown.

(e) Green/red ratio of granules as in (d), just prior to exocytosis, and separated for events with (flash) or without flash (FF). n, number of events.

(f) As in (e), but in for exocytosis events in presence of 10 mM NH_4^+. Values for flash and FF in e-f were not significantly different. n, number of events.

Figure 5 – Figure supplement 2: Activation of SUR1 by tolbutamide does not affect fusion pore restriction.

(a) Image sequences of a granule undergoing K^+-stimulated exocytosis in an INS-1 cell expressing NPY-tdmOrange2 and EGFP-SUR1.

(b) Quantification of GFP-SUR1 binding to the granule site (ΔF/S) in presence (green) or absence (black) of tolbutamide.

(c) Exocytosis (40 s K^+) in cells as in (a), separated for restricted fusion pores (flash events, in color) and full fusion events (in white); the decrease with tolbutamide was significant (P=0.001); n, number of cells.

(d) Percentage of flash events in cells expressing EGFP-SUR, with or without tolbutamide.

Figure 6 – Figure supplement 1: NPY and amisyn/dynamin1 recruitment profiles at the point of release

(a) Exocytosis events separated for flashes (left, green) and full fusions (right, grey) for dynamin1-GFP and NPY-tdmOrange2 expressing INS-1 cells in presence of forskolin from Fig 6. n, number of events

(b) As in a, but for mCherry-amisyn and NPY EGFP expressing INS-1 cells from Fig 6. n, number of events

(c) As in a, but in absence of forskolin. n, number of events

(d) As in b, but in absence of forskolin. n, number of events

Figure 6 – Figure supplement 2: Quantification of overexpression. Ins1-cells expressing mCherry-amisyn or dynamin1-GFP were fixated and immunostained using anti-amisyn or anti-dynamin1 and fluorescence was quantified for both labels by TIRFM of single cells.

(a) example images of immunostaining (upper) and mCherry-amisyn (lower).

(b) average fluorescence (cell-background) for immunostaining (white) and mCherry-amisyn (grey).

(c) Plot of mCherry-amisyn vs immunostaining fluorescence; each symbol represents one cell. The offset at the y-axis corresponds to cells that only express endogenous amisyn.

(d-e) as b-c but for dynamin1.

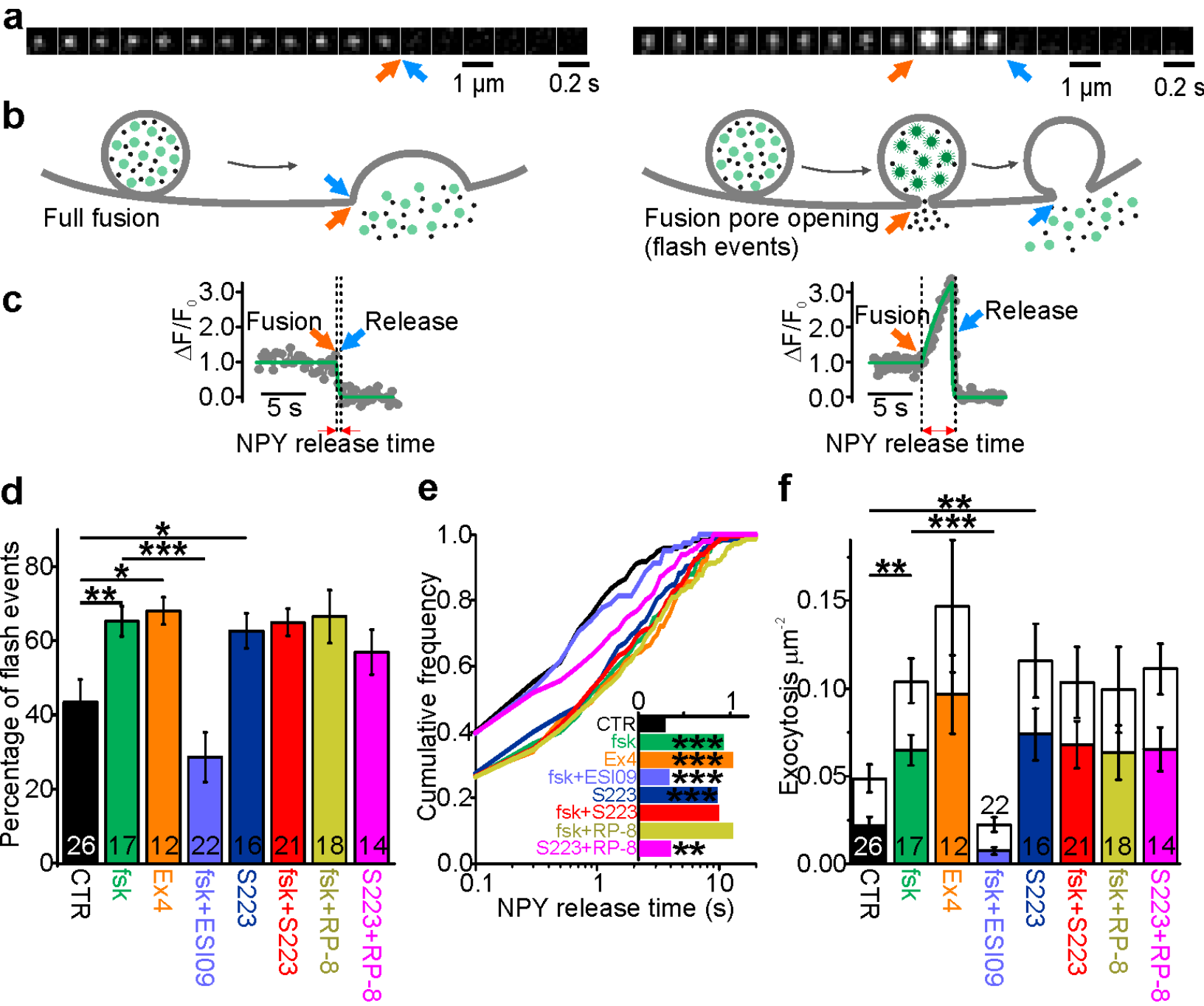
a
1 µm
0.2 s
1 µm
0.2 s
b
Full fusion
Fusion pore opening
(flash events)
c
ΔF/F0
3.0
2.0
1.0
0.0
Fusion
Release
5 s
NPY release time
ΔF/F0
3.0
2.0
1.0
0.0
Fusion
Release
5 s
NPY release time
d
Percentage of flash events
80
60
40
20
0
*
***
*
**
26
17
12
22
16
21
18
14
CTR
fsk
Ex4
fsk+ESI09
S223
fsk+S223
fsk+RP-8
S223+RP-8
e
Cumulative frequency
1.0
0.8
0.6
0.4
0.2
0.0
0.1
1
10
NPY release time (s)
0
1
CTR
fsk
***
Ex4
***
fsk+ESI09
***
S223
***
fsk+S223
fsk+RP-8
S223+RP-8
**
f
Exocytosis µm-2
0.15
0.10
0.05
0.00
**
***
**
22
26
17
12
16
21
18
14
CTR
fsk
Ex4
fsk+ESI09
S223
fsk+S223
fsk+RP-8
S223+RP-8

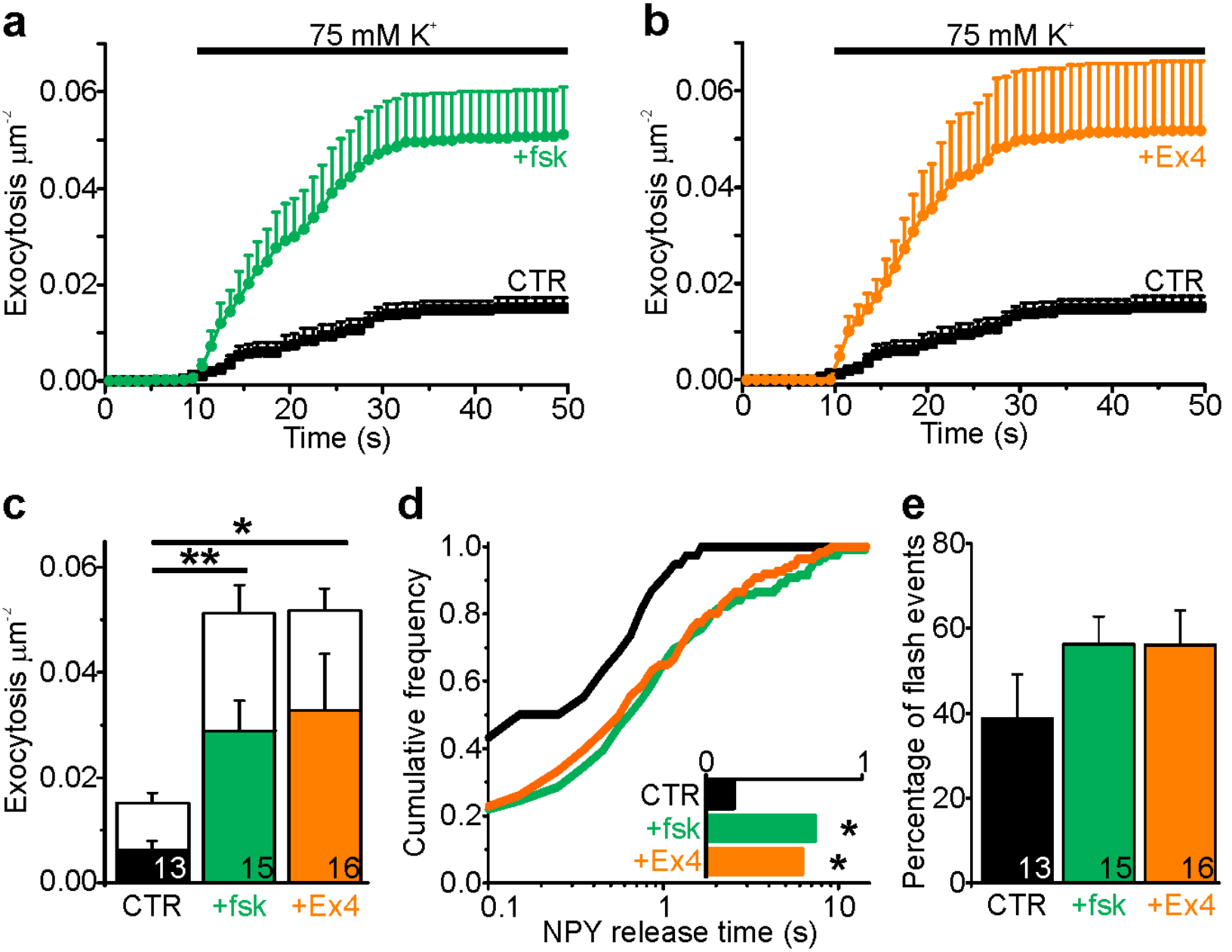
a
75 mM K+
Exocytosis µm-2
0.06
0.04
0.02
0.00
+fsk
CTR
0
10
20
30
40
50
Time (s)
b
75 mM K+
Exocytosis µm-2
0.06
0.04
0.02
0.00
+Ex4
CTR
0
10
20
30
40
50
Time (s)
c
*
**
Exocytosis µm-2
0.06
0.04
0.02
0.00
13
15
16
CTR
+fsk
+Ex4
d
Cumulative frequency
1.0
0.8
0.6
0.4
0.2
0.0
0
1
CTR
+fsk
+Ex4
*
*
0.1
1
10
NPY release time (s)
e
Percentage of flash events
80
60
40
20
0
13
15
16
CTR
+fsk
+Ex4

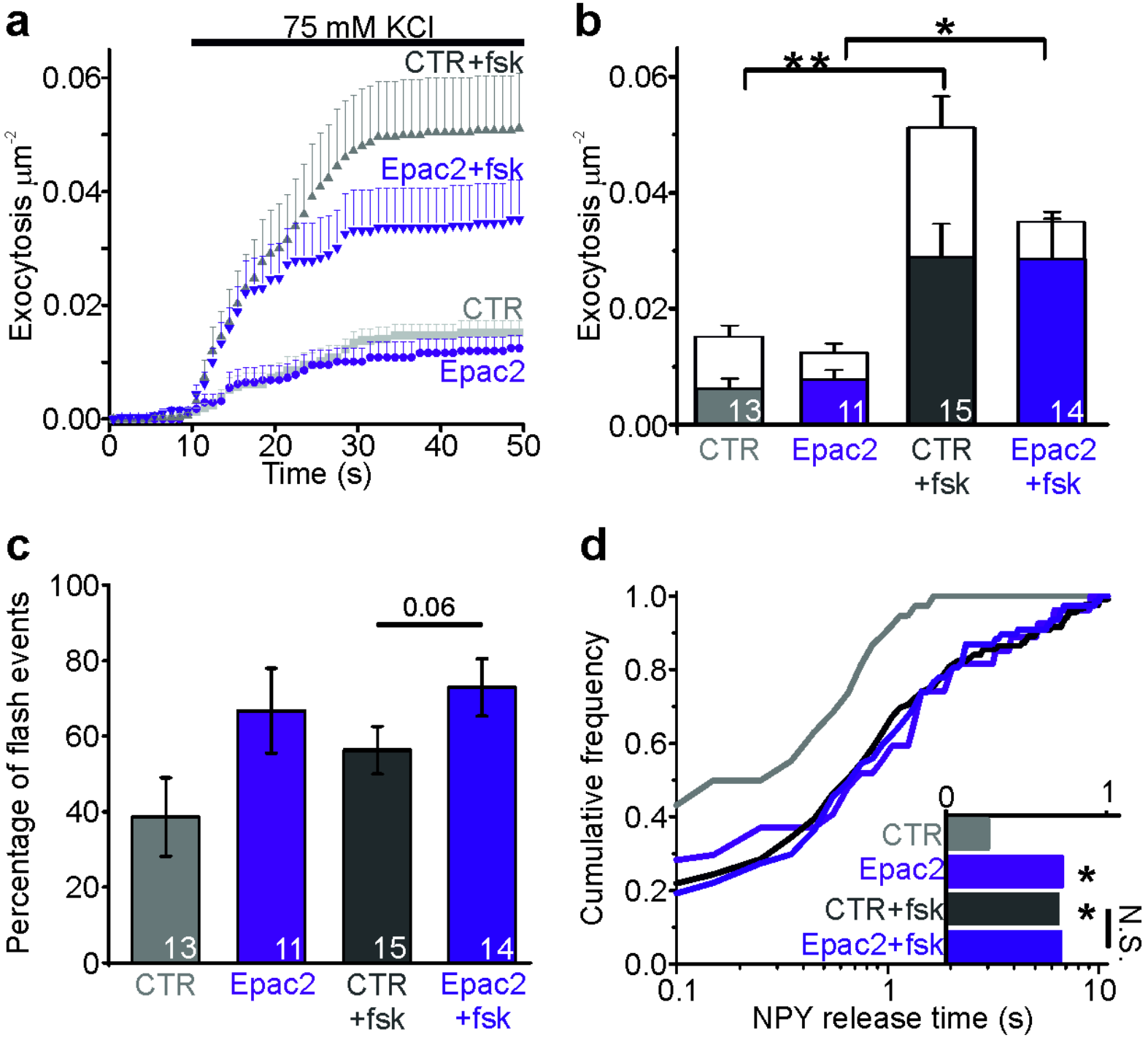
a
75 mM KCl
CTR+fsk
Epac2+fsk
CTR
Epac2
Exocytosis µm-2
0.06
0.04
0.02
0.00
0
10
20
30
40
50
Time (s)
b
**
*
Exocytosis µm-2
0.06
0.04
0.02
0.00
13
11
15
14
CTR
Epac2
CTR +fsk
Epac2 +fsk
c
Percentage of flash events
100
80
60
40
20
0
0.06
13
11
15
14
CTR
Epac2
CTR +fsk
Epac2 +fsk
d
Cumulative frequency
1.0
0.8
0.6
0.4
0.2
0.0
0.1
1
10
NPY release time (s)
0
1
CTR
Epac2
*
CTR+fsk
*
Epac2+fsk
N.S.

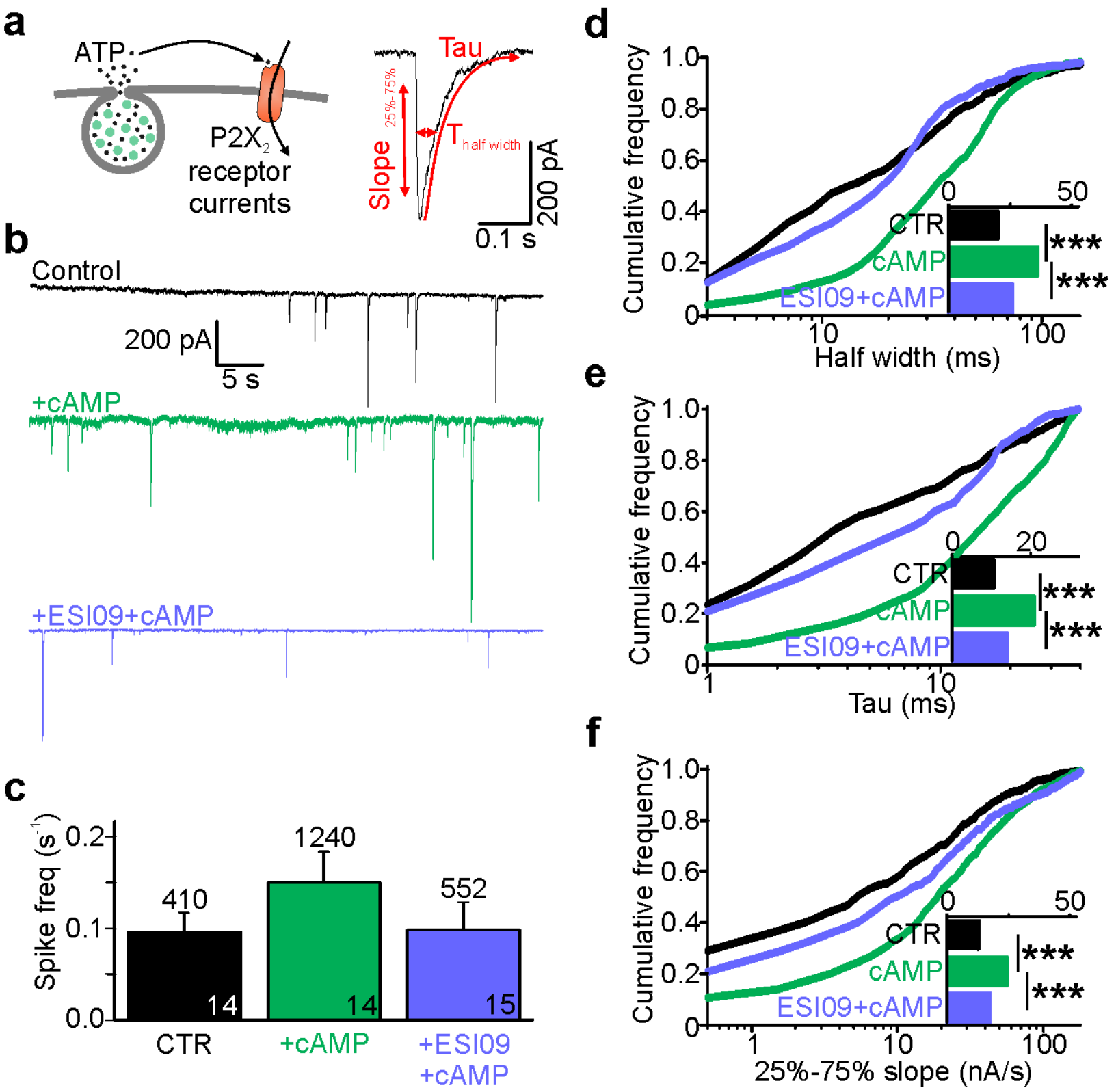
a
ATP
P2X2
receptor
currents
Tau
Slope 25%-75%
T half width
200 pA
0.1 s
b
Control
200 pA
5 s
+cAMP
+ESI09+cAMP
c
Spike freq (s-1)
0.2
0.1
0.0
410
1240
552
14
14
15
CTR
+cAMP
+ESI09
+cAMP
d
Cumulative frequency
1.0
0.8
0.6
0.4
0.2
0
0
50
CTR
cAMP
ESI09+cAMP
***
***
10
100
Half width (ms)
e
Cumulative frequency
1.0
0.8
0.6
0.4
0.2
0
0
20
CTR
cAMP
ESI09+cAMP
***
***
1
10
Tau (ms)
f
Cumulative frequency
1.0
0.8
0.6
0.4
0.2
0
0
50
CTR
cAMP
ESI09+cAMP
***
***
1
10
100
25%-75% slope (nA/s)

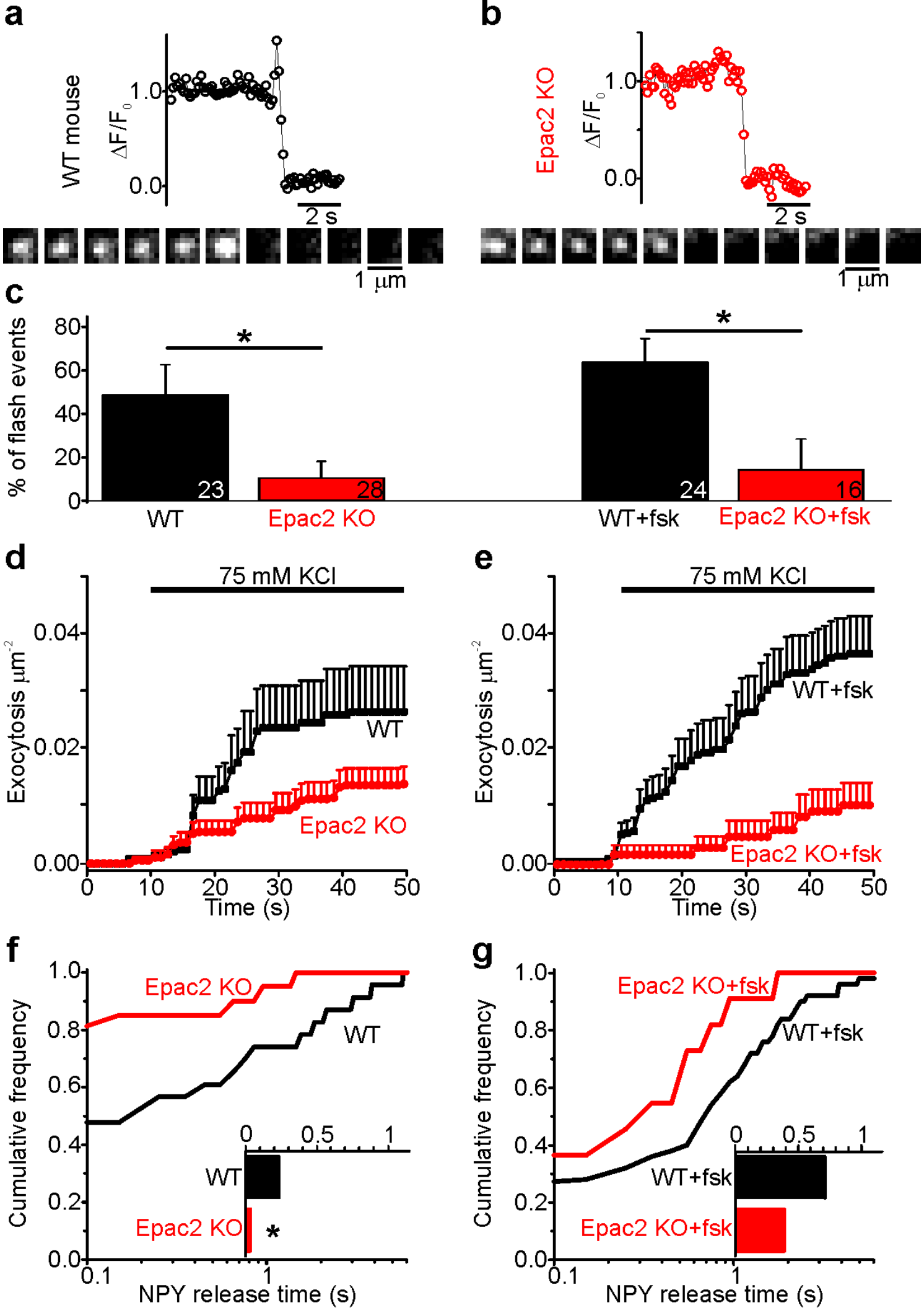
a
WT mouse
ΔF/F0
1.0
0.0
2 s
1 μm
b
Epac2 KO
ΔF/F0
1.0
0.0
2 s
1 μm
c
% of flash events
80
60
40
20
0
*
*
23
28
24
16
WT
Epac2 KO
WT+fsk
Epac2 KO+fsk
d
75 mM KCl
Exocytosis μm-2
0.04
0.02
0.00
WT
Epac2 KO
0
10
20
30
40
50
Time (s)
e
75 mM KCl
Exocytosis μm-2
0.04
0.02
0.00
WT+fsk
Epac2 KO+fsk
0
10
20
30
40
50
Time (s)
f
Cumulative frequency
1.0
0.8
0.6
0.4
0.2
0.0
Epac2 KO
WT
0
0.5
1
WT
Epac2 KO
*
0.1
1
NPY release time (s)
g
Cumulative frequency
1.0
0.8
0.6
0.4
0.2
0.0
Epac2 KO+fsk
WT+fsk
0
0.5
1
WT+fsk
Epac2 KO+fsk
0.1
1
NPY release time (s)

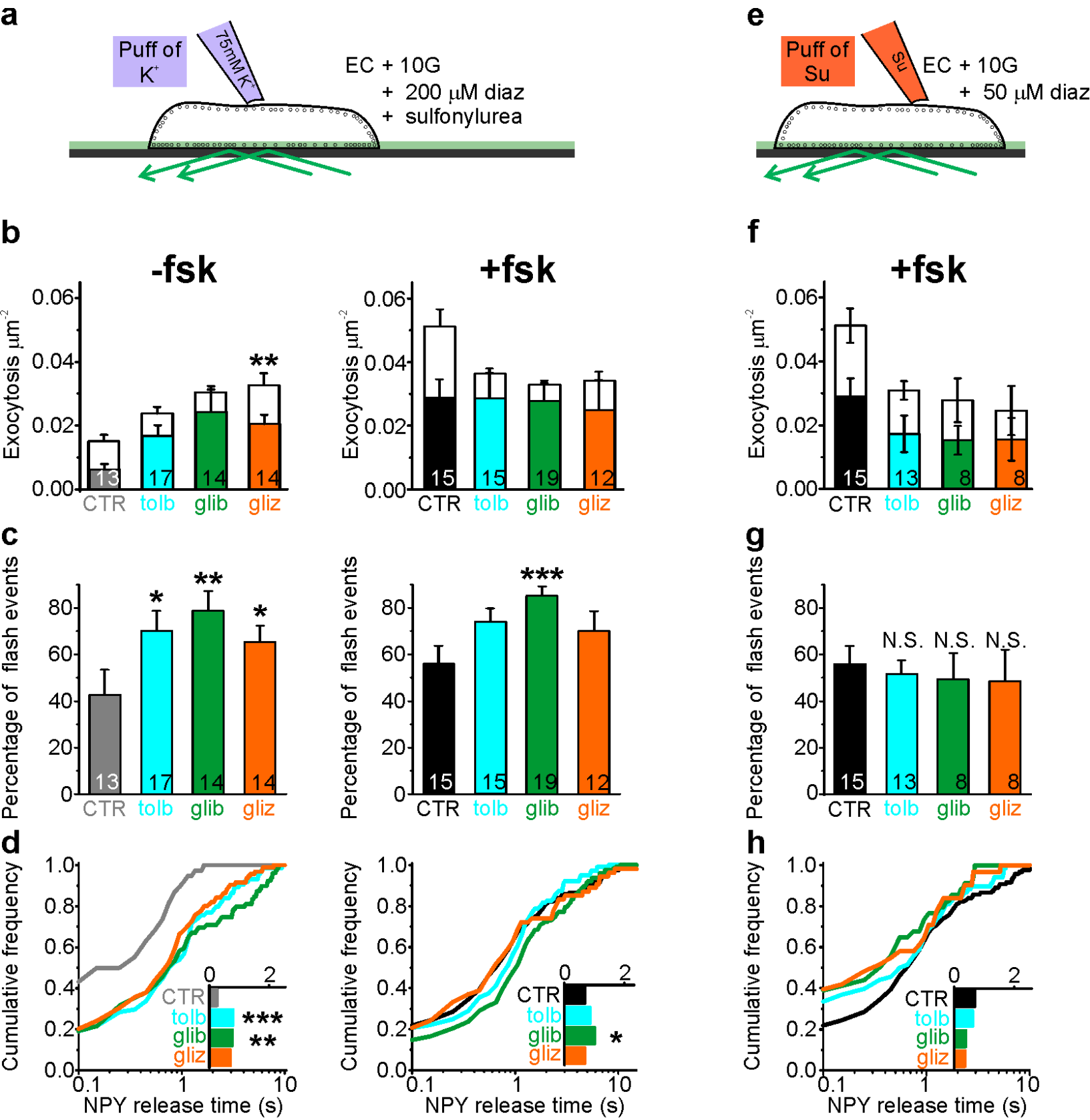
a
Puff of K+
75mM K+
EC + 10G
+ 200 μM diaz
+ sulfonylurea
e
Puff of Su
Su
EC + 10G
+ 50 μM diaz
b
-fsk
+fsk
Exocytosis μm-2
0.06
0.04
0.02
0.00
**
13
17
14
14
15
15
19
12
CTR
tolb
glib
gliz
f
+fsk
15
13
8
8
c
Percentage of flash events
80
60
40
20
0
*
**
*
***
g
N.S.
d
Cumulative frequency
1.0
0.8
0.6
0.4
0.2
0.0
0.1
1
10
NPY release time (s)
0
2
***
**
h

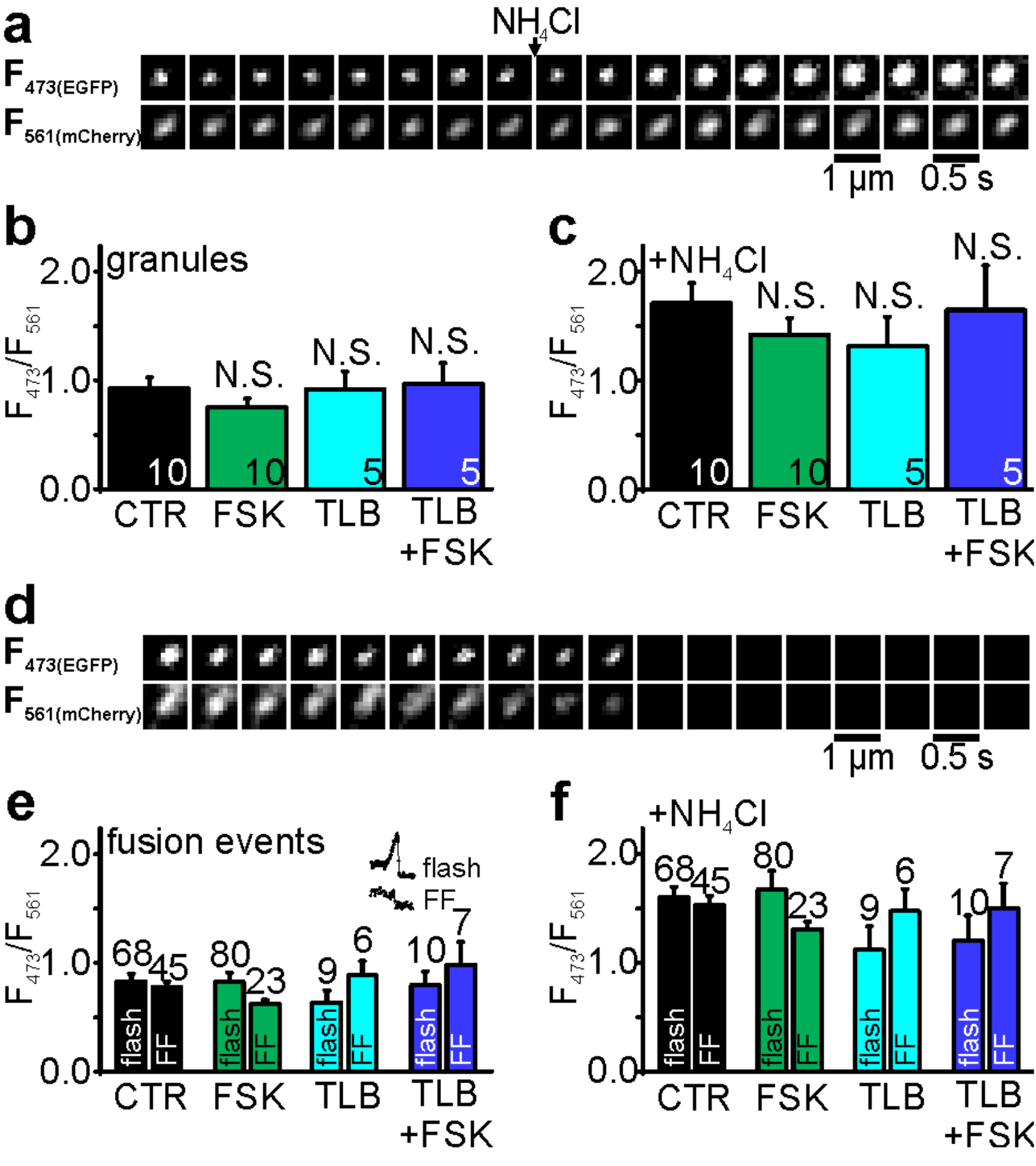
a
NH4Cl
F473(EGFP)
F561(mCherry)
1 µm
0.5 s
b
granules
F473/F561
2.0
1.0
0.0
N.S.
N.S.
N.S.
10
10
5
5
CTR
FSK
TLB
TLB +FSK
c
+NH4Cl
N.S.
N.S.
N.S.
d
e
fusion events
flash
FF
68
45
80
23
9
6
10
7
f
+NH4Cl

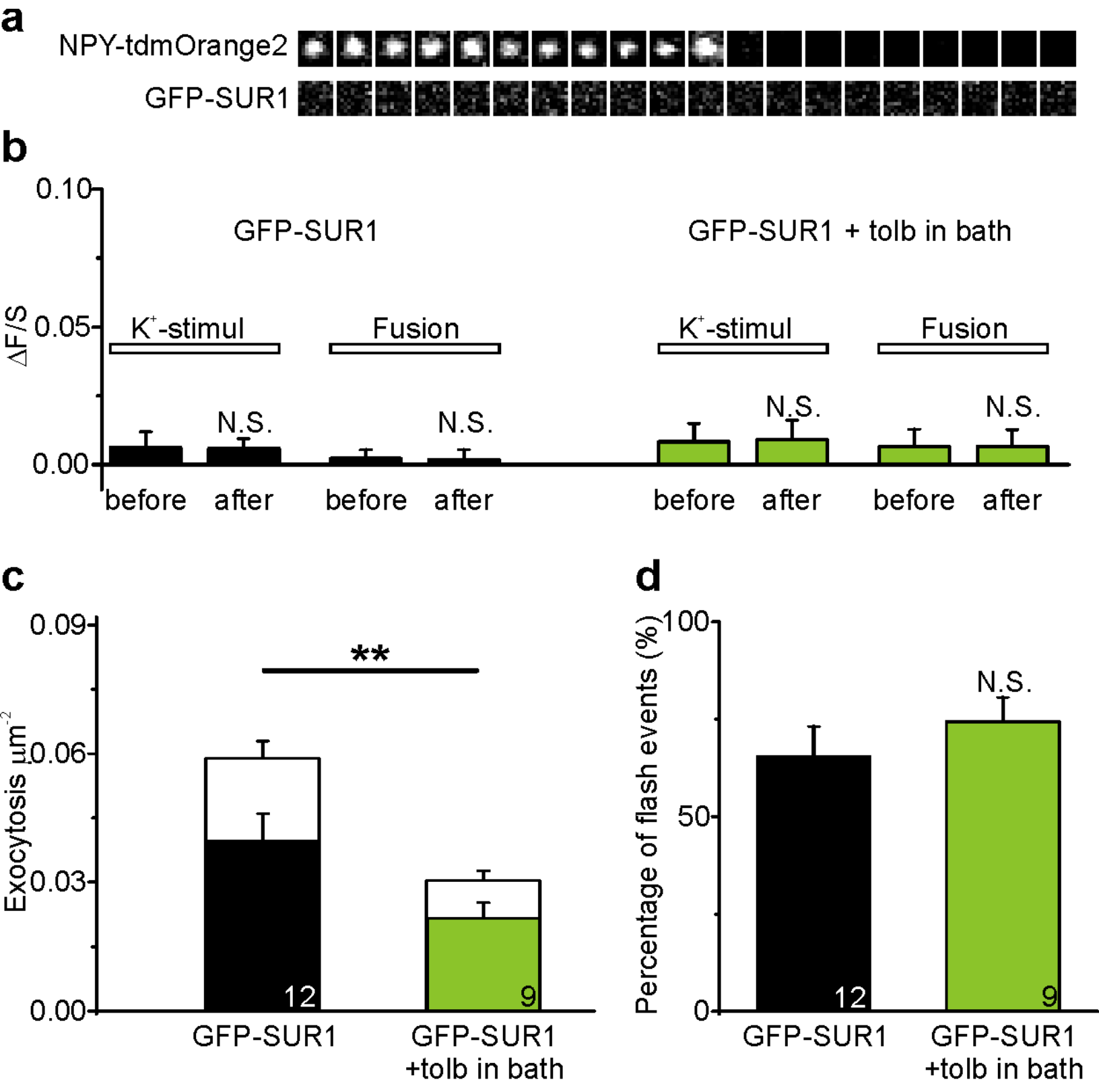
a
NPY-tdmOrange2
GFP-SUR1
b
0.10
0.05
0.00
ΔF/S
GFP-SUR1
GFP-SUR1 + tolb in bath
K+-stimul
Fusion
K+-stimul
Fusion
N.S.
N.S.
N.S.
N.S.
before
after
before
after
before
after
before
after
c
0.09
0.06
0.03
0.00
Exocytosis µm-2
**
12
9
GFP-SUR1
GFP-SUR1 +tolb in bath
d
100
50
0
Percentage of flash events (%)
N.S.
12
9
GFP-SUR1
GFP-SUR1 +tolb in bath

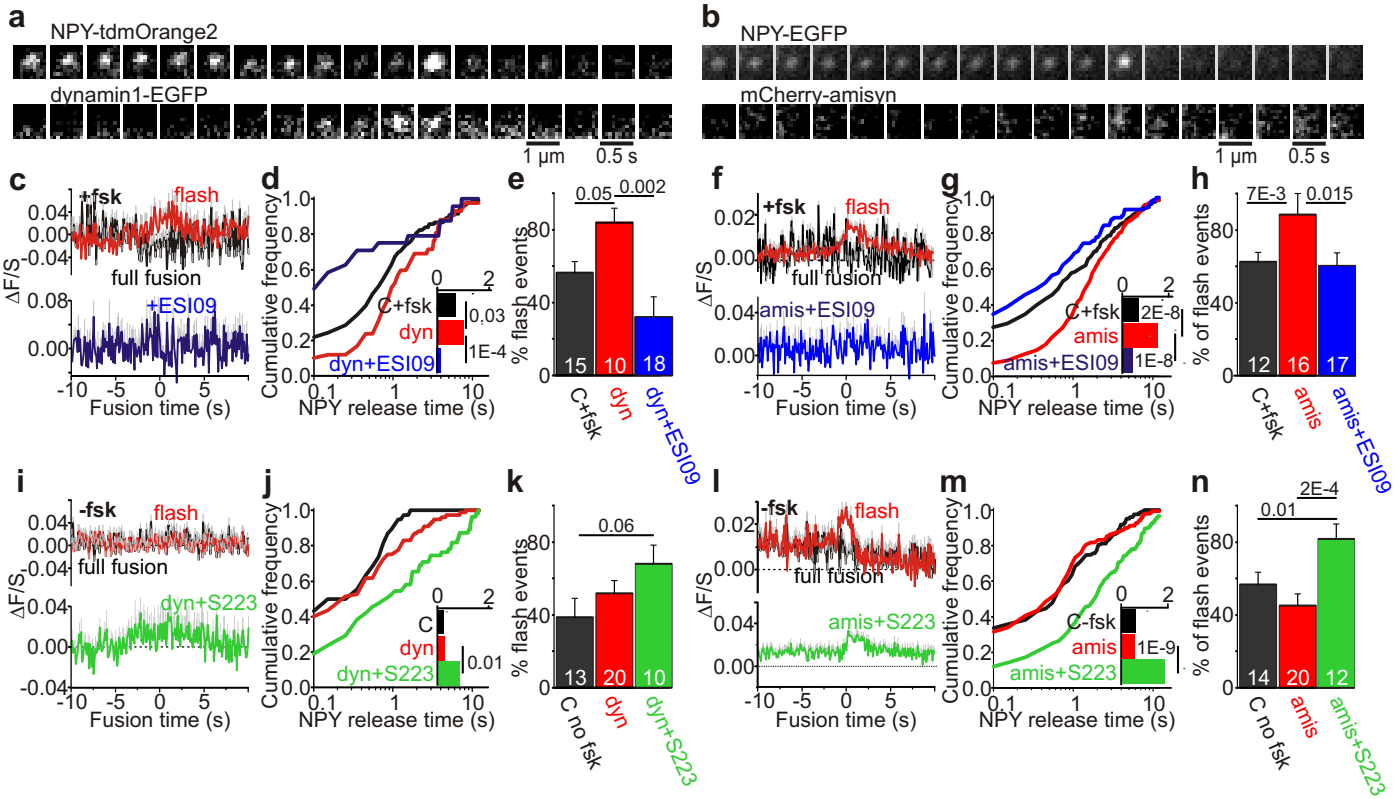
a
NPY-tdmOrange2
dynamin1-EGFP
1 µm
0.5 s
b
NPY-EGFP
mCherry-amisyn
1 µm
0.5 s
c
+fsk
flash
full fusion
+ESI09
ΔF/S
Fusion time (s)
d
Cumulative frequency
C+fsk
dyn
dyn+ESI09
NPY release time (s)
e
% flash events
0.05
0.002
15
10
18
C+fsk
dyn
dyn+ESI09
f
+fsk
flash
full fusion
amis+ESI09
ΔF/S
Fusion time (s)
g
Cumulative frequency
C+fsk
amis
amis+ESI09
NPY release time (s)
h
% of flash events
7E-3
0.015
12
16
17
C+fsk
amis
amis+ESI09
i
-fsk
flash
full fusion
dyn+S223
ΔF/S
Fusion time (s)
j
Cumulative frequency
C
dyn
dyn+S223
NPY release time (s)
k
% flash events
0.06
13
20
10
C no fsk
dyn
dyn+S223
l
-fsk
flash
full fusion
amis+S223
ΔF/S
Fusion time (s)
m
Cumulative frequency
C-fsk
amis
amis+S223
NPY release time (s)
n
% of flash events
2E-4
0.01
14
20
12
C no fsk
amis
amis+S223

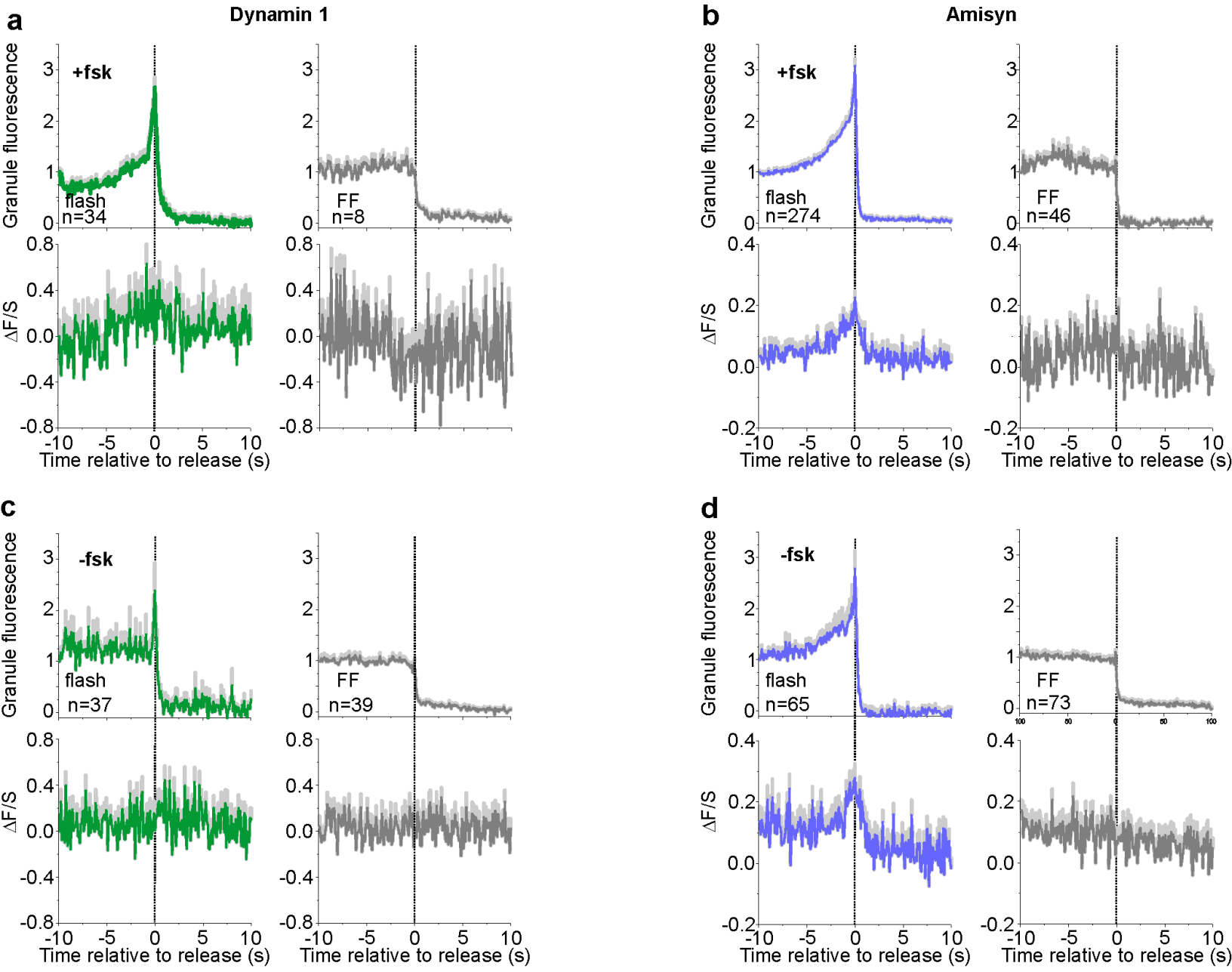
a
Dynamin 1
b
Amisyn
+fsk
flash
n=34
FF
n=8
flash
n=274
FF
n=46
-fsk
flash
n=37
FF
n=39
flash
n=65
FF
n=73
Granule fluorescence
ΔF/S
Time relative to release (s)
c
d

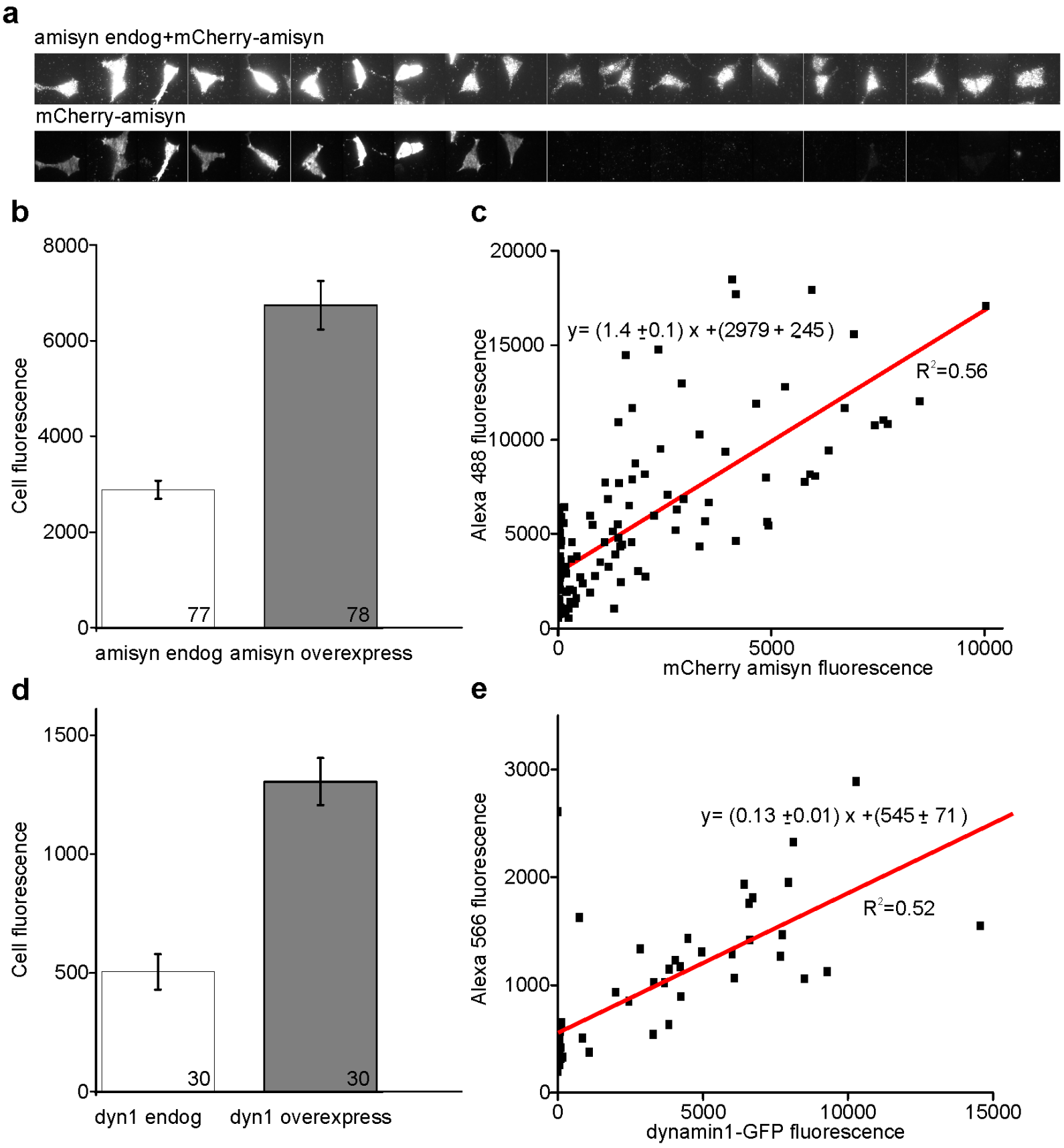
a
amisyn endog+mCherry-amisyn
mCherry-amisyn
b
8000
6000
4000
2000
0
Cell fluorescence
77
78
amisyn endog
amisyn overexpress
c
20000
15000
10000
5000
0
Alexa 488 fluorescence
y= (1.4 ±0.1) x +(2979 ± 245)
R2=0.56
0
5000
10000
mCherry amisyn fluorescence
d
1500
1000
500
0
Cell fluorescence
30
30
dyn1 endog
dyn1 overexpress
e
3000
2000
1000
0
Alexa 566 fluorescence
y= (0.13 ±0.01) x +(545 ± 71)
R2=0.52
0
5000
10000
15000
dynamin1-GFP fluorescence

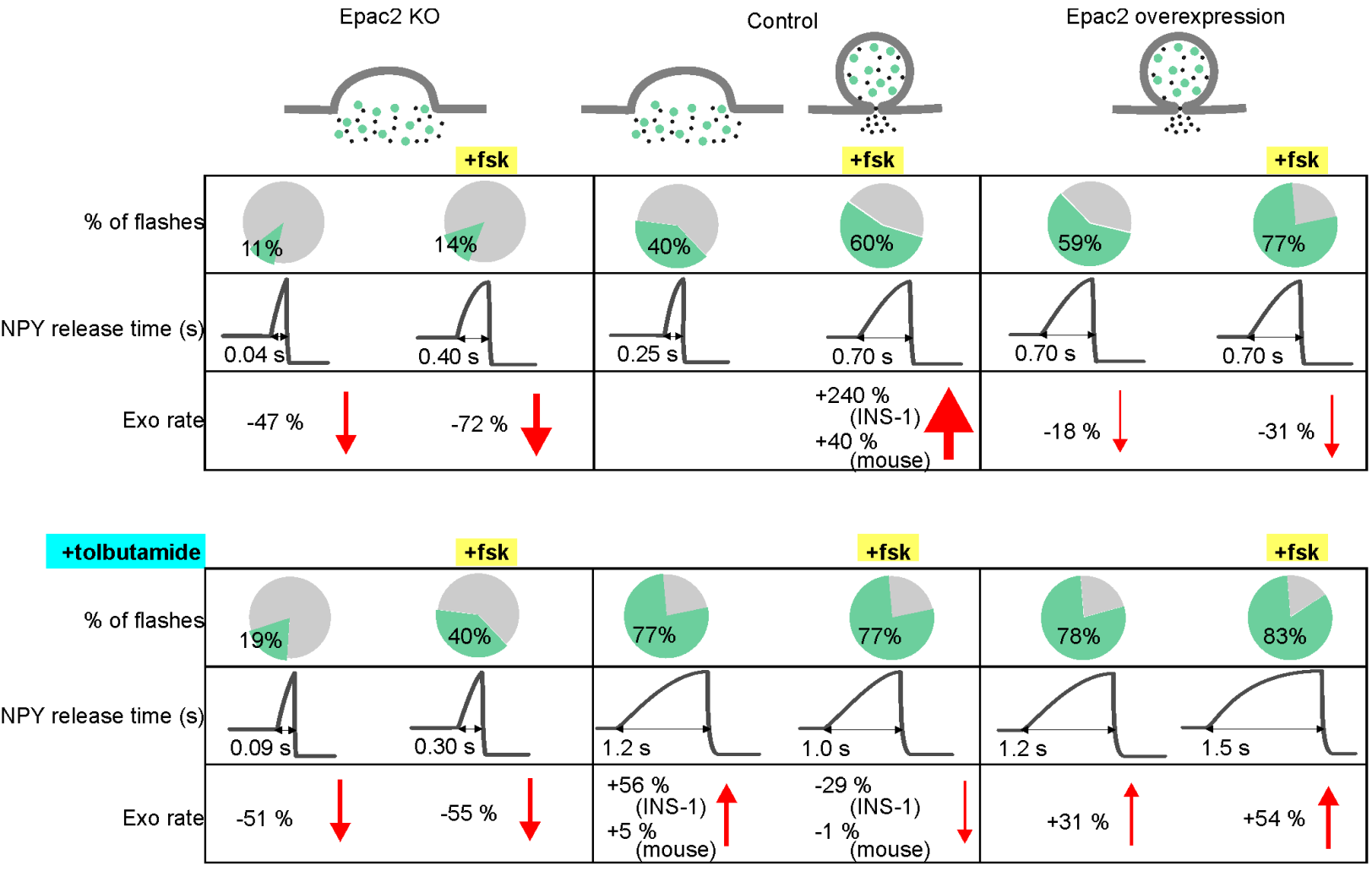
Epac2 KO
Control
Epac2 overexpression
+fsk
+fsk
+fsk
% of flashes
11%
14%
40%
60%
59%
77%
NPY release time (s)
0.04 s
0.40 s
0.25 s
0.70 s
0.70 s
0.70 s
Exo rate
-47 %
-72 %
+240 %
(INS-1)
+40 %
(mouse)
-18 %
-31 %
+tolbutamide
+fsk
+fsk
+fsk
% of flashes
19%
40%
77%
77%
78%
83%
NPY release time (s)
0.09 s
0.30 s
1.2 s
1.0 s
1.2 s
1.5 s
Exo rate
-51 %
-55 %
+56 %
(INS-1)
+5 %
(mouse)
-29 %
(INS-1)
-1 %
(mouse)
+31 %
+54 %